



# Report

## Statistical Loads Data For The Airbus A-320 Aircraft In Commercial Operations

.....

December 2001

John W. Rustenburg  
Donald A. Skinn  
Daniel O. Tipps

---

1. Report No. DOT/FAA/AR		2. Government Accession No.		3. Recipient's Catalog No.	
4. Title and Subtitle STATISTICAL LOADS DATA FOR THE AIRBUS A-320 AIRCRAFT IN COMMERCIAL OPERATIONS				6. Performing Organization Code	
7. Author(s) John W. Rustenburg, Donald A. Skinn, and Daniel O. Tipps				8. Performing Organization Report No. UDR-TR-2001-00080	
9. Performing Organization Name and Address University of Dayton Research Institute Structural Integrity Division 300 College Park Dayton, OH 45469-0120				10. Work Unit No. (TRAIS) RPD-510	
				11. Contract or Grant No. Grant No. 00-G-015	
12. Sponsoring Agency Name and Address U.S. Department of Transportation Federal Aviation Administration Office of Aviation Research Washington, DC 20591				13. Type of Report and Period Covered Final Report	
				14. Sponsoring Agency Code	
15. Supplementary Notes The Federal Aviation Administration William J. Hughes Technical Center COTR was Thomas DeFiore					
16. Abstract <p>The primary objective of this research is to develop new and improved methods and criteria for processing and presenting large commercial transport airplane flight and ground loads usage data. The scope of activities performed involves (1) defining the service-related factors that affect the operational life of commercial aircraft; (2) designing an efficient software system to reduce, store, and process large quantities of optical quick-access recorder data; and (3) reducing, analyzing, and providing processed data in statistical formats that will enable the FAA to reassess existing certification criteria. Equally important, these new data will also enable the FAA, the aircraft manufacturers, and the airlines to better understand and control those factors that influence the structural integrity of commercial transport aircraft. Presented herein are Airbus A-320 aircraft operational usage data collected from 10,066 flights, representing 30,817 flight hours, as recorded by a single U.S. airline operator. Statistical data are presented on the aircraft's usage, flight and ground loads data, and systems operational data. The data presented in this report will provide the user with information about the accelerations, speeds, altitudes, flight duration and distance, gross weights, speed brake/spoiler cycles, thrust reverser usage, and gust velocities encountered by the Airbus A-320 during actual operational usage.</p>					
17. Key Words Optical quick access recorder, Flight profiles, Flight loads, Ground loads, Systems operational data, Statistical loads data			18. Distribution Statement This document is available to the public through the National Technical Information Service (NTIS), Springfield, Virginia 22161.		
19. Security Classif. (of this report) Unclassified		20. Security Classif. (of this page) Unclassified		21. No. of Pages	22. Price N/A

## PREFACE

The Flight Systems Integrity Group of the Structural Integrity Division of the University of Dayton Research Institute (URDI) performed this work under Federal Aviation Administration (FAA) Grant No. 00-G-015 entitled "An Assessment of A-320 Operational Loads and Usage Characteristics and Automated Systems Effects." The Program Manager for the FAA was Mr. Thomas DeFiore of the FAA William J. Hughes Technical Center at Atlantic City International Airport, New Jersey, and the Program Technical Advisor was Mr. Terence Barnes of the FAA Aircraft Certification Office. Mr. Daniel Tipps was the Principal Investigator for the University of Dayton, provided overall technical direction for this effort, and assisted in preparation of the final report. Mr. Donald Skinn developed the data reduction algorithms, programmed the data reduction criteria, and performed the data reduction. Mr. John Rustenburg performed the data analysis, created the graphical presentations, and assisted in preparation of the final report.

While UDRI tries to use the same data reduction criteria when processing data from different aircraft types, there are circumstances when the criteria must be revised in order to accurately retrieve data associated with a desired event. Specifically, when the squat switch indication was used on the Airbus A-320 as the criteria to determine when liftoff and touchdown occurred, the processed data showed that the squat switch did not provide an accurate indication of when these events actually occurred. Thus, UDRI conducted a study to determine if a better criteria could be developed for determining when these events occurred. The new criteria, which were developed, used radio altitude to identify when liftoff occurred and time (5-seconds) prior to when the squat switch indication came on to identify when touchdown occurred.

The application of these new criteria provided good results, but all statistical data involving the A-320 aircraft operations during liftoff and touchdown that had been previously processed had to be redone. Of particular importance, when the new touchdown criteria were used, it was discovered that the vertical load factor data associated with the touchdown event had been previously processed as having occurred during the approach phase of flight phase instead of at touchdown. Consequently, the previously processed gust velocity flight data reflected the response to occurrences of vertical load factors that should have been attributed to landing impact.

Based on these findings from the A-320 program, UDRI looked at the statistical data it had previously processed at touchdown for other aircraft types such as the B-737, MD-80, and B-767, and concluded that the new criteria for touchdown could affect the data presented in published reports for those aircraft. Thus, the statistical data presented in those reports may need to be updated using the new touchdown criteria. It is also possible that the gust velocity data contained in some of the earlier FAA/NASA documents could be affected by UDRI's findings. A list of these reports is shown on the next page.

## TABLE OF CONTENTS

	Page
EXECUTIVE SUMMARY	xi
1. INTRODUCTION	1
2. AIRCRAFT DESCRIPTION	1
3. AIRLINE DATA COLLECTION AND EDITING SYSTEMS	3
3.1 Airline Data Collection System	3
3.2 Airline Data Editing System	4
4. UNIVERSITY OF DAYTON RESEARCH INSTITUTE DATA PROCESSING	4
4.1 Recorded Data Parameters	4
4.2 Computed Parameters	5
4.2.1 Atmospheric Density	5
4.2.2 Equivalent Airspeed	5
4.2.3 Dynamic Pressure ( $q$ )	6
4.2.4 Derived Gust Velocity ( $U_{de}$ )	6
4.2.5 Continuous Gust Intensity ( $U_{\sigma}$ )	7
4.2.6 Flight Distance	8
4.2.7 Rate of Climb	8
4.3 Data Reduction Operations	8
4.3.1 Initial Quality Screening	8
4.3.2 Time History Files	9
4.3.3 Relational Database	10
4.3.4 Permanent Data Files	10
4.3.5 Loads Data Reduction	11
4.4 Data Reduction Criteria	11
4.4.1 Phases of Flight Profile	11
4.4.1.1 Ground Phases	12
4.4.1.2 Airborne Phases	12
4.4.2 Specific Events	13
4.4.2.1 Liftoff	14

## APPENDICES

A – Data Presentation

B – Great Circle Distance Calculation

## LIST OF SYMBOLS AND ABBREVIATIONS

$\bar{A}$	aircraft PSD gust response factor
$a$	speed of sound (ft/sec)
$a_0$	speed of sound at sea level (ft/sec)
$\bar{c}$	wing mean geometric chord (ft)
$\bar{C}$	aircraft discrete gust response factor
$C_{L_\alpha}$	aircraft lift curve slope per radian
$C_{L_{\max}}$	maximum lift coefficient
$CAS$	calibrated air speed
$c.g.$	center of gravity
$D$	integrated flight distance
$EAS$	equivalent airspeed
$F(PSD)$	continuous gust alleviation factor
$g$	gravity constant, 32.17 ft/sec <sup>2</sup>
$H_p$	pressure altitude, (ft)
$K_g$	discrete gust alleviation factor, $0.88 \mu / (5.3 + \mu)$
$KCAS$	knots calibrated air speed
$KEAS$	knots equivalent air speed
$kts$	knots
$L$	turbulence scale length (ft)
$M$	Mach number
$M_{MO}$	Maximum Mach number at altitude
$N$	number of occurrences for $U_\sigma$ (PSD gust procedure)
$N_0$	number of zero crossings per nautical mile (PSD gust procedure)
$N_1$	fan (low pressure compressor) rotor speed (percentage of normal maximum turbine speed.)
$N_2$	turbine (high pressure compressor) rotor speed (percentage of normal maximum turbine speed)
$nm$	nautical mile
$n_x$	longitudinal load factor (g)
$n_y$	lateral load factor (g)
$n_z$	vertical load factor (g)

LIST OF AIRPORT CODES

ABQ	ALBUQUERQUE	MCO	ORLANDO
ACA	ACAPULCO	MEX	MEXICO CITY
AMA	AMARILLO	MIA	MIAMI
ATL	ATLANTA	MRY	MONTEREY
AUS	AUSTIN	MSN	MADISON
BDL	WINDSOR LOCKS	MSP	MINNEAPOLIS
BIL	BILLINGS	MSY	NEW ORLEANS
BNA	NASHVILLE	OAK	OAKLAND
BOS	BOSTON	OMA	OMAHA
BUF	BUFFALO	ONT	ONTARIO
BWI	BALTIMORE	ORD	CHICAGO
CCS	CARACAS	ORF	NORFOLK
CLE	CLEVELAND	PDX	PORTLAND
CLT	CHARLOTTE	PHL	PHILADELPHIA
CMH	COLUMBUS	PHX	PHOENIX
COS	COLORADO SPRINGS	PIT	PITTSBURGH
CVG	COVINGTON/CINCINNATI	PVD	PROVIDENCE
CYVR	VANCOUVER	RDU	RALEIGH/DURHAM
DCA	WASHINGTON NATIONAL	RFD	ROCKFORD
DEN	DENVER	RIC	RICHMOND
DFW	DALLAS/FORT WORTH	RNO	RENO
DSM	DES MOINES	SAL	SAN SALVADOR
DTW	DETROIT	SAN	SAN DIEGO
EWR	NEWARK	SEA	SEATTLE
GRR	GRAND RAPIDS	SFO	SAN FRANCISCO
GSO	GREENSBORO	SJC	SAN JOSE
GXY	GREELEY	SJO	SAN JOSE
IAD	WASHINGTON DULLES	SJU	SAN JUAN
IAH	HOUSTON	SLC	SALT LAKE CITY
IDA	IDAHO FALLS	SMF	SACRAMENTO
IND	INDIANAPOLIS	SNA	SANTA ANA (ORANGE CITY)
JAC	JACKSON	STL	ST LOUIS
JFK	NEW YORK	STT	ST THOMAS
LAS	LAS VEGAS	TPA	TAMPA
LAX	LOS ANGELES	TUL	TULSA
LGA	NEW YORK	TUS	TUCSON
LNK	LINCOLN	YYC	CALGARY
MCI	KANSAS CITY	YYZ	TORONTO INTERNATIONAL

## EXECUTIVE SUMMARY

The primary objective of this research is to develop new and improved methods and criteria for processing and presenting large commercial transport airplane flight and ground loads usage data. The scope of activities performed involves (1) defining the service-related factors that affect the operational life of commercial aircraft; (2) designing an efficient software system to reduce, store, and process large quantities of optical quick-access recorder data; and (3) reducing, analyzing, and providing processed data in statistical formats that will enable the FAA to reassess existing certification criteria. Equally important, these new data will also enable the FAA, the aircraft manufacturers, and the airlines to better understand and control those factors that influence the structural integrity of commercial transport aircraft. Presented herein are Airbus A-320 aircraft operational usage data collected from 10,066 flights, representing 30,817 flight hours, as recorded by a single U.S. airline operator. Statistical data are presented on the aircraft's usage, flight and ground loads data, and systems operations. The data presented in this report will provide the user with information about the accelerations, speeds, altitudes, flight duration and distance, gross weights, speed brake/spoiler cycles, thrust reverser usage, and gust velocities encountered by the Airbus A-320 during actual operational usage.

## 1. INTRODUCTION.

The Federal Aviation Administration (FAA) has an ongoing airborne data monitoring systems research program to collect, process, and evaluate statistical flight and ground loads data from transport aircraft used in normal commercial airline operations. The objectives of this program are (a) to acquire, evaluate, and utilize typical operational in-service data for comparison with the prior data used in the design and qualification testing of civil transport aircraft and (b) to provide a basis to improve the structural criteria and methods of design, evaluation, and substantiation of future airplanes. The University of Dayton Research Institute (UDRI) supports the FAA's efforts by developing the technology for reducing, processing, analyzing, and reporting on the operational flight and ground loads data received from the airlines participating in the FAA program and by conducting research studies.

Since the inception of the FAA's Airborne Data Monitoring Systems Research Program, the scope of the Flight Loads Program has steadily expanded to include research on data collected from several aircraft operators and on aircraft models such as the B-737, B-767, MD-82/83, and BE-1900D. While current program research efforts are tailored primarily to support the FAA and the aircraft structural design community in evaluating design criteria related to the strength, durability, and damage tolerance of the basic airframe structure, much of the data that are available, when provided in meaningful statistical formats, can provide the aircraft operator with some valuable insight into how his aircraft and aircraft systems are being used during normal flight and ground operations. In an effort to improve the data content and to disseminate meaningful data to the larger community of designers, regulators, and aircraft operators, UDRI has made changes, deletions, and additions to the statistical data formats as presented in past reports. These changes occur throughout the data presentation section of this report.

This report presents flight and ground loads data obtained from 56 Airbus A-320 aircraft representing 10,066 flights and 30,817 hours of airline operations from one U.S. carrier.

## 2. AIRCRAFT DESCRIPTION.

The Airbus A-320 is the first subsonic commercial aircraft equipped with fly-by-wire control throughout the entire flight envelope, and the first aircraft to have sidestick controls instead of the standard control column and aileron wheel. The fly-by-wire system controls ailerons, elevators, spoilers, flaps, leading-edge devices, engine thrust, and rudder and tail surface trim. The flight control system incorporates a feature that will not allow the aircraft's structural and aerodynamic limits to be exceeded regardless of pilot input.

Table 1 presents certain operational characteristics and major physical dimensions of the Airbus A-320 aircraft, and figure 1 presents a three-view drawing showing front, top, and side views of the aircraft.

### 3. AIRLINE DATA COLLECTION AND EDITING SYSTEMS.

The airline data collection and editing system consists of two major components: (1) the data collection system installed on board the aircraft and (2) the ground data editing station. A schematic overview of the system is shown in figure 2. The data collection and editing systems are discussed in more detail below.

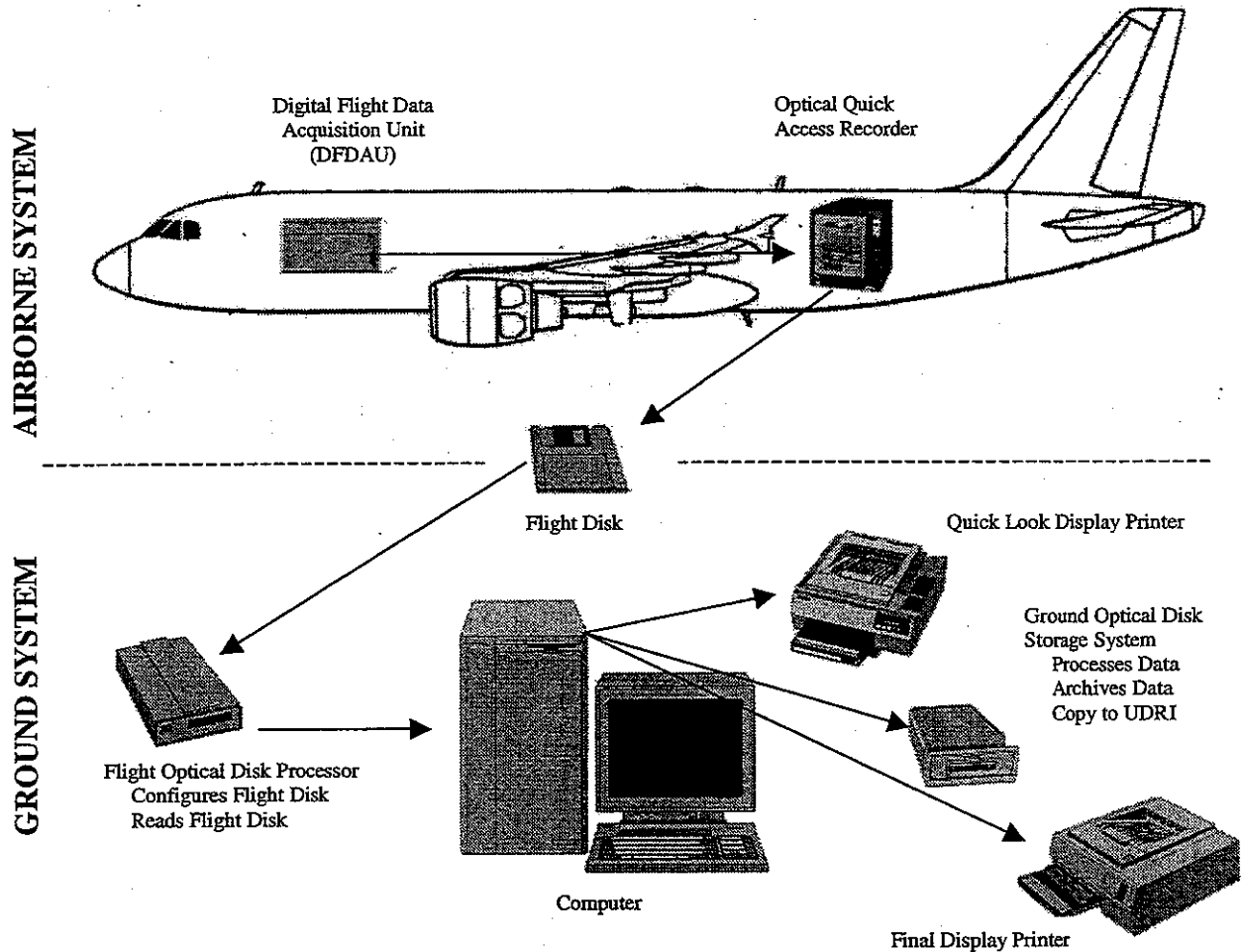


FIGURE 2. AIRLINE RECORDING AND EDITING SYSTEM

#### 3.1 Airline Data Collection System.

The onboard data collection system for the Airbus A-320 consists of a Digital Flight Data Acquisition Unit (DFDAU), a Digital Flight Data Recorder (DFDR), and an Optical Quick-Access Recorder (OQAR). The DFDAU collects sensor signals and sends parallel data signals to both the DFDR and the OQAR. The OQAR is equipped with an optical disk, which can store up to 300 hours of flight data, whereas the DFDR uses a 25-hour looptape. The optical disk is periodically removed from the OQAR and forwarded to the ground processing station.

However, not all parameters listed in table 2 are used for statistical analysis and data presentation. Those recorded parameters that are used by UDRI to create time history files, compressed onto MO disks, and processed through the data reduction software for statistical analysis and data presentation are highlighted in table 2.

#### 4.2 Computed Parameters.

Certain information and parameters needed in subsequent data reduction are not recorded and need to be extracted or derived from available time history data. Derived gust velocity,  $U_{de}$ , and continuous gust intensity,  $U_{\sigma}$ , are important statistical load parameters, which are derived from measured vertical accelerations. This derivation of  $U_{de}$  and  $U_{\sigma}$  requires knowledge of atmospheric density, equivalent airspeed, and dynamic pressure. These values are calculated using equations that express the rate of change of density as a function of altitude based on the International Standard Atmosphere.

##### 4.2.1 Atmospheric Density.

For altitudes below 36,089 feet, the density  $\rho$  is expressed as a function of altitude by

$$\rho = \rho_0 (1 - 6.876 \times 10^{-6} \times H_p)^{4.256} \quad (1)$$

where  $\rho_0$  is air density at sea level (0.0023769 slugs/ft<sup>3</sup>) and  $H_p$  is pressure altitude (ft). Pressure altitude is a recorded parameter.

##### 4.2.2 Equivalent Airspeed.

Equivalent air speed ( $V_e$ ) is a function of true air speed ( $V_T$ ) and the square root of the ratio of air density at altitude ( $\rho$ ) to air density at sea level ( $\rho_0$ ) and is expressed as

$$V_e = V_T \sqrt{\frac{\rho}{\rho_0}} \quad (2)$$

True airspeed ( $V_T$ ) is derived from Mach number ( $M$ ) and speed of sound ( $a$ ):

$$V_T = Ma \quad (3)$$

Mach number is dimensionless and is a recorded parameter. The speed of sound ( $a$ ) is a function of pressure altitude ( $H_p$ ) and the speed of sound at sea level and is expressed as

$$a = a_0 \sqrt{(1 - 6.876 \times 10^{-6} \times H_p)} \quad (4)$$

Substituting equations 1 and 4 into equation 2 gives

$$V_e = M \times a_0 \times (1 - 6.876 \times 10^{-6} \times H_p)^{0.5} \times (1 - 6.876 \times 10^{-6} \times H_p)^{2.128} \quad (5)$$

#### 4.2.5 Continuous Gust Intensity ( $U_\sigma$ ).

Power spectral density (PSD) functions provide a turbulence description in terms of the probability distribution of the root-mean-square (rms) gust velocities. The root-mean-square gust velocities or continuous gust intensities,  $U_\sigma$ , are computed from the peak gust value of vertical acceleration using the power spectral density technique as described in reference 1 as

$$U_\sigma = \frac{\Delta n_z}{A} \quad (10)$$

where  $\Delta n_z$  = gust peak incremental vertical acceleration

$$\bar{A} = \text{aircraft PSD gust response factor} = \frac{\rho_0 V_e C_{L\alpha} S}{2W} F(\text{PSD}) \text{ in } \frac{1}{\text{ft/sec}} \quad (11)$$

$\rho_0$  = 0.002377 slugs/ft<sup>3</sup>, standard sea level air density

$V_e$  = equivalent airspeed (ft/sec)

$C_{L\alpha}$  = aircraft lift-curve slope per radian

$S$  = wing reference area (ft<sup>2</sup>)

$W$  = gross weight (lbs)

$$F(\text{PSD}) = \frac{11.8}{\sqrt{\pi}} \left[ \frac{\bar{c}}{2L} \right]^{\frac{1}{3}} \sqrt{\frac{\mu}{110 + \mu}}, \text{ dimensionless} \quad (12)$$

$\bar{c}$  = wing mean geometric chord (ft)

$L$  = turbulence scale length, 2500 ft

$$\mu = \frac{2W}{\rho g \bar{c} C_{L\alpha} S}, \text{ dimensionless} \quad (13)$$

$\rho$  = air density (slugs/ft<sup>3</sup>)

$g$  = 32.17 ft/sec<sup>2</sup>

To determine the number of occurrences ( $N$ ) for  $U_\sigma$ , calculate

$$N = \frac{N_0(o)_{ref}}{N_0(o)} = \frac{\pi \bar{c}}{203} \left[ \frac{\rho}{\rho_0} \mu \right]^{0.46}, \text{ dimensionless} \quad (14)$$

where  $\bar{c}$ ,  $\rho$ ,  $\rho_0$ , and  $\mu$  are defined above. Then each  $U_\sigma$  peak is counted as  $N$  counts at that  $U_\sigma$  value. This number of counts is used to determine the number of counts per nautical mile ( $nm$ ), or

$$\frac{\text{counts}}{nm} = \left( \frac{N}{\text{distance flown in counting interval}} \right) \quad (15)$$

Finally, the number of such counts is summed from the largest plus or minus value toward the smallest to produce the cumulative counts per nautical mile.

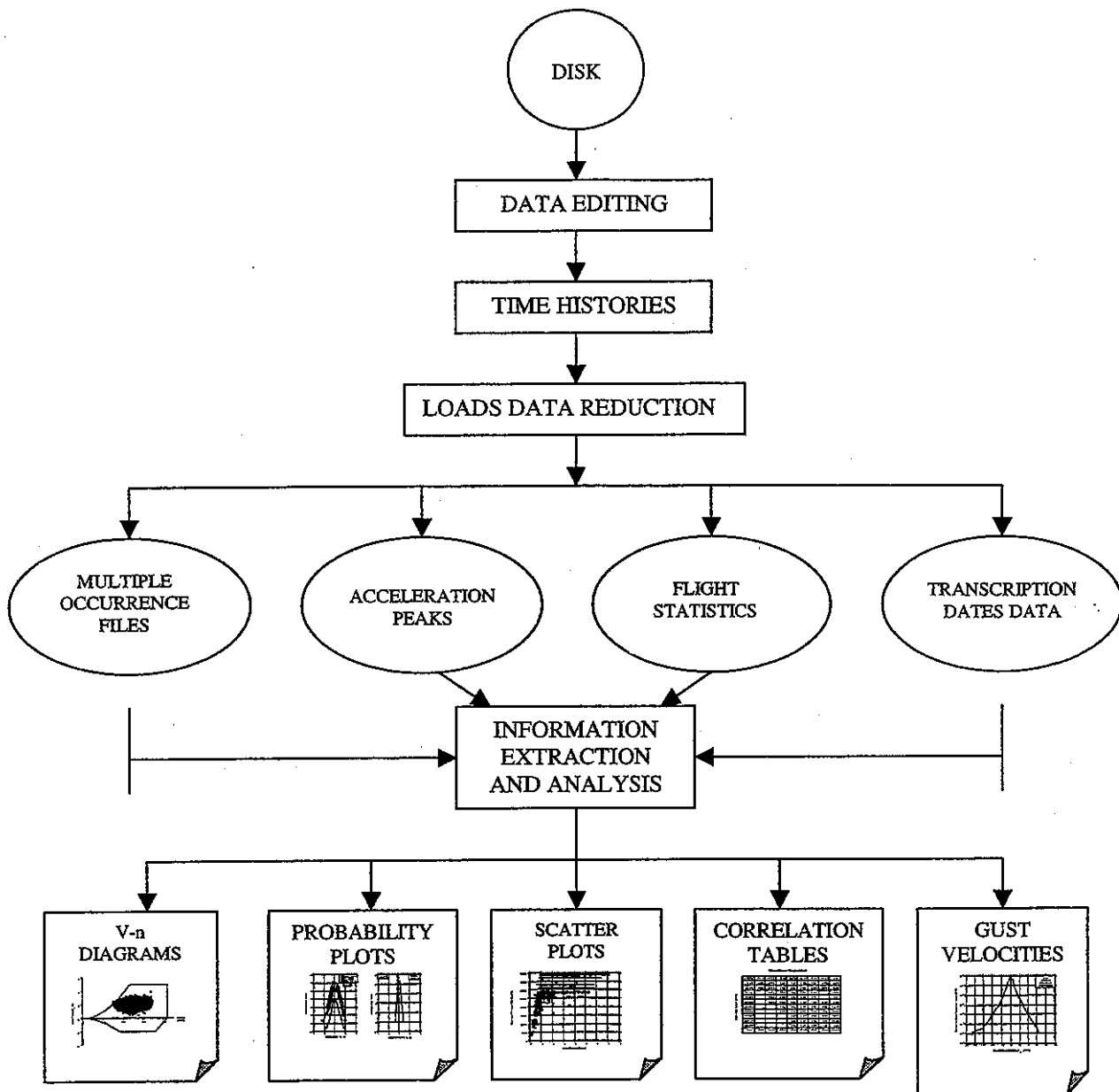


FIGURE 3. DATA PROCESSING FLOW CHART

#### 4.3.2 Time History Files.

Each magneto-optical disk provided by the airline contains multiple flights for each airplane. The files on MO disks are separated into individual parameter time history files for each flight. Then these time history files are compressed and stored on the same 230-MB magneto-optical disks for later recall by the flight loads processing software. Data editing and verification are performed on the data as the time histories are being prepared. Message alerts indicate that obviously erroneous data have been removed and/or that questionable data have been retained but need to be manually reviewed prior to their acceptance. Table 3 lists the limits against which the data are compared. Some of the parameters from table 1 are edited and retained even though they are not currently being used.

#### 4.3.5 Loads Data Reduction.

The loads data reduction program uses the compressed time history files to derive statistical information on aircraft usage, ground loads, flight loads, and systems operations. These data are then reduced in accordance with specific data reduction criteria.

#### 4.4 Data Reduction Criteria.

To process the measured data into statistical loads formats, specific data reduction criteria were developed for separating the phases of ground and flight operations, identifying specific events associated with operation of the aircraft and its onboard systems, assigning sign conventions, determining maximum and minimum values and load cycles, and distinguishing between gust and maneuver load factors. These criteria are discussed in the following paragraphs.

##### 4.4.1 Phases of Flight Profile.

The ground and flight phases were determined by UDRI from the recorded data. Each time history profile was divided into nine phases—four ground phases (taxi out, takeoff roll, landing roll with and without thrust reverser deployed, and taxi in) and five airborne phases (departure, climb, cruise, descent, and approach). Figure 4 shows these nine phases of a typical flight profile.

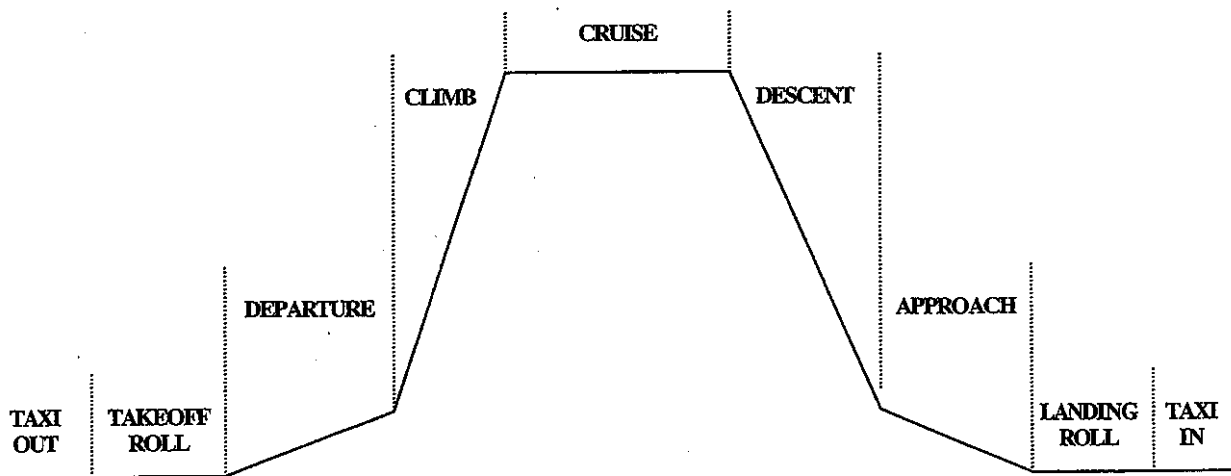


FIGURE 4. DESCRIPTION OF FLIGHT PROFILE PHASES

The criteria used to define each of these phases are summarized in table 4 and discussed in more detail in the following paragraphs.

off at liftoff until it turns on again at landing touchdown. The beginning of each flight phase is defined based on combinations of the squat switch position, flap settings, and/or the calculated rate of climb or descent over a period of at least 1 minute as shown in table 4. Also, by definition, the departure phase cannot be less than 1 minute in length.

It should be noted that an airborne phase could occur several times per flight because it is determined by the rate of climb and the position of the flaps. When this occurs, the flight loads data are combined and presented as a single flight phase. The UDRI software then creates a file that chronologically lists the phases of flight and their corresponding starting times.

4.4.2 Specific Events.

In addition to the ground and airborne phases, a unique set of criteria was also required to identify certain specific events such as liftoff, landing touchdown, thrust reverser deployment and stowage, and start and completion of turnoff from the active runway after landing. Figure 5 shows a sketch depicting these phases and events.

The criteria used to define each of the specific events are summarized in table 5 and discussed in more detail in reference 2 and the following paragraphs.

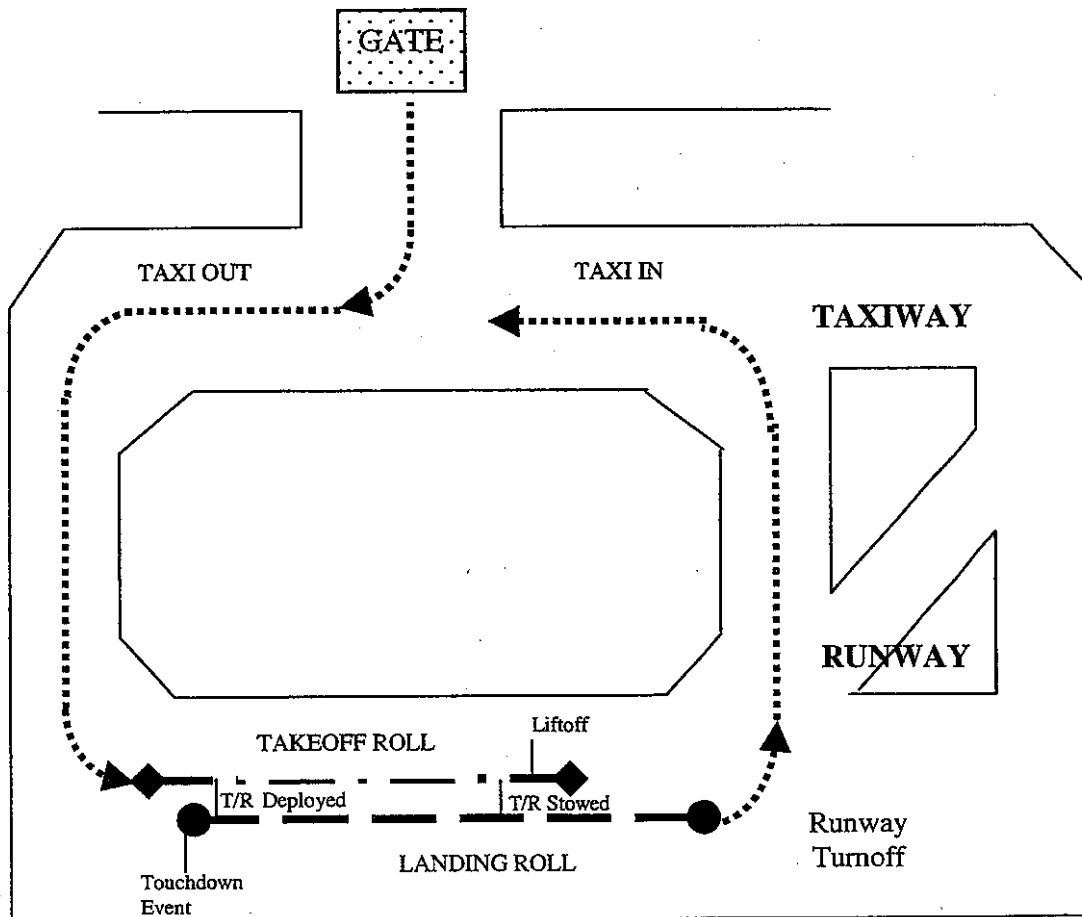


FIGURE 5. SKETCH OF GROUND PHASES AND SPECIFIC EVENTS

subsequent magnetic heading readings were averaged and this average heading was defined as the runway centerline. Subsequent magnetic heading changes were then tested to identify continuous movement in the same direction away from this centerline. When the aircraft's sequential magnetic heading change exceeded 13.5 degrees from the direction of the landing centerline, the time slice associated with the first sequential heading change from the landing centerline in the direction of the turn was defined as the beginning of the turnoff from the runway.

An alternate method was used to identify flights involving "shallow" turns from the runway that did not exceed the 13.5 degree turn criteria. This method uses aircraft ground speed and magnetic heading to calculate the aircraft's position relative to the runway centerline by identifying when the aircraft's position perpendicular to the runway centerline exceeded 100 feet. The time slice associated with the first aircraft movement away from the landing centerline in the direction of the turn was defined as the beginning of the aircraft's turnoff from the runway.

The end point of the first turnoff from the active runway was also identified using magnetic heading readings. An algorithm was developed that uses the changes in magnetic heading, while the aircraft was in its turn, to identify when the aircraft had either returned to taxiing in a straight line or was turning in the opposite direction. The first point that provided this indication was then defined as the end point of the turnoff from the runway. This point is also the beginning of the taxi in phase.

#### 4.4.3 Sign Conventions.

Acceleration data are recorded in three directions: vertical (z), lateral (y), and longitudinal (x). As shown in figure 6, the positive z direction is up; the positive y direction is airplane starboard; and the positive x direction is forward.

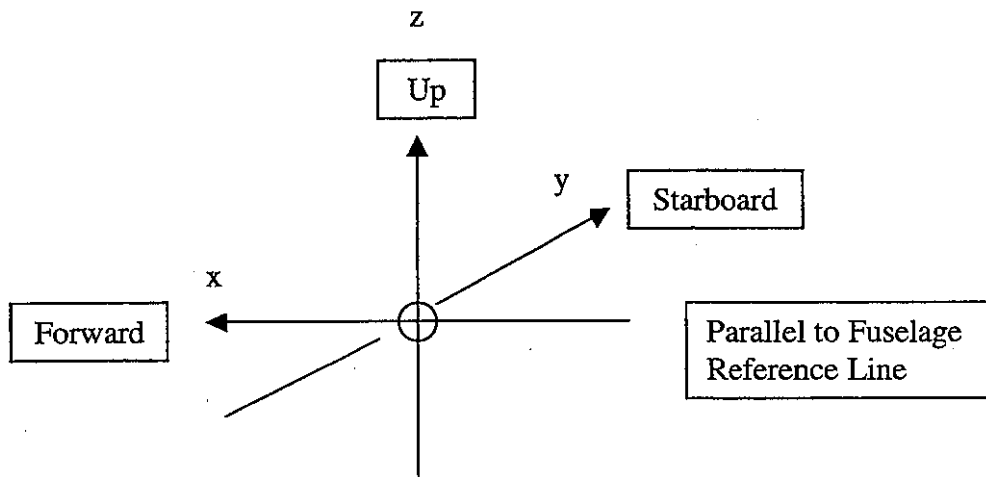


FIGURE 6. SIGN CONVENTION FOR AIRPLANE ACCELERATIONS

#### 4.4.5 Separation of Maneuver and Gust Load Factors.

Vertical acceleration,  $n_z$ , is measured at the center of gravity (c.g.) of the aircraft and incremental vertical acceleration,  $\Delta n_z$ , results from removing the 1-g condition from  $n_z$ . The incremental acceleration measured at the c.g. of the aircraft in flight may be the result of either maneuvers or gusts. In order to derive gust and maneuver statistics, the maneuver-induced acceleration ( $\Delta n_{z_{man}}$ ) and the gust response acceleration ( $\Delta n_{z_{gust}}$ ) must be separated from the total acceleration history. Reference 3 reported the results of a UDRI study to evaluate methods of separating maneuver and gust load factors from measured acceleration time histories. As a result of this study, UDRI uses a cycle duration rule to differentiate maneuver-induced acceleration peaks from those peaks caused by gust loading. Review of the A-320 response characteristics has shown that a cycle duration of 2.0 seconds is appropriate for the A-320 aircraft and thus was used.

#### 4.4.6 Flap Detents.

When flaps are extended, the effective deflection is considered to be that of the applicable detent, as indicated in table 6. The flap deflection ranges and placard speeds reflect the flap operational limits, as provided by Airbus Industries 15 June 1999.

TABLE 6. FLAP DETENTS (AIRBUS A-320)

Flap Detent	Minimum Flap Setting	Maximum Flap Setting	Operational Airspeed Limit (KCAS)
0	0	0	230
10	> 0	≤ 10	215
15	> 10	≤ 15.3	200
20	> 15.3	≤ 20	185
40	> 20	≤ 40	177

### 5. DATA PRESENTATION.

The statistical data presented in this section provide the FAA, aircraft manufacturers, and the operating airline with the information that is needed to assess how the A-320 aircraft is actually being used in operational service versus its original design or intended usage. The statistical data presented herein can be used by the FAA as a basis to evaluate existing structural certification criteria, to improve requirements for the design, evaluation, and substantiation of existing aircraft, and to establish design criteria for future generations of new aircraft. The aircraft manufacturer can use these data to assess the aircraft's structural integrity by comparing the actual in-service usage of the A-320 aircraft versus its originally intended design usage. It can also use these data to derive typical flight profiles and to update structural strength, durability, and damage tolerance analyses in order to establish or revise maintenance and inspection requirements for critical airframe and structural components. The airline/aircraft operator can use these data to evaluate the aircraft's current usage with respect to established operational procedures and placard limitations. It can also use these data to identify where changes in current operational procedures could provide additional safety margins, increase the service life of structural components, and improve on the economics of its operations.

TABLE 7. STATISTICAL DATA FORMATS (CONT'D.)

Data Description	Figure
Cumulative Frequency of Incremental Vertical Load Factor During Landing Roll	A-36
Maximum Incremental Vertical Load Factor vs. Maximum Angle of Attack During Lift off, 130-140 Knots	A-37
Maximum Incremental Vertical Load Factor vs. Maximum Angle of Attack During Lift off, 140-150 Knots	A-38
Maximum Incremental Vertical Load Factor vs. Maximum Angle of Attack During Lift off, 150-160 Knots	A-39
Maximum Incremental Vertical Load Factor vs. Maximum Angle of Attack During Lift off, 160-170 Knots	A-40
Maximum Incremental Vertical Load Factor vs. Maximum Angle of Attack During Lift off, 170-180 knots	A-41
Maximum Incremental Vertical Load Factor vs. Maximum Angle of Attack During Lift off, 180-190 knots	A-42
Maximum Incremental Vertical Load Factor at Touchdown vs. Maximum Yaw Angle Before Touchdown	A-43
Maximum Incremental Vertical Load Factor at Touchdown vs. Mean Yaw Angle Before Touchdown	A-44
Maximum Incremental Vertical Load Factor at Touchdown vs. Maximum Bank Angle Before Touchdown	A-45
Maximum Incremental Vertical Load Factor at Touchdown vs. Mean Wind Speed Before Touchdown	A-46
Maximum Incremental Vertical Load Factor at Touchdown vs. Mean Inertial Vertical Velocity Before Touchdown	A-47
Maximum Incremental Vertical Load Factor vs. Coincident Airspeed at Touchdown	A-48
Aircraft Runway Acceleration Response	A-49
<b>FLIGHT LOADS DATA</b>	
<b>GUST VERTICAL LOAD FACTOR DATA</b>	
Cumulative Occurrences of Incremental Vertical Gust Load Factor per 1000 Hours by Flight Phase	A-50
Cumulative Occurrences of Incremental Vertical Gust Load Factor per 1000 Hours, Combined Flight Phases	A-51
Cumulative Occurrences of Incremental Vertical Gust Load Factor per Nautical Mile by Flight Phase	A-52
Cumulative Occurrences of Incremental Vertical Gust Load Factor per Nautical Mile, Combined Flight Phases	A-53
<b>DERIVED GUST VELOCITY DATA</b>	
Cumulative Occurrences of Derived Gust Velocity per Nautical Mile, < 500 Feet Above Airport	A-54
Cumulative Occurrences of Derived Gust Velocity per Nautical Mile, 500-1,500 Feet Above Airport	A-55
Cumulative Occurrences of Derived Gust Velocity per Nautical Mile, < 500 Feet	A-56
Cumulative Occurrences of Derived Gust Velocity per Nautical Mile, 500-1,500 Feet	A-57
Cumulative Occurrences of Derived Gust Velocity per Nautical Mile, 1,500-4,500 Feet	A-58
Cumulative Occurrences of Derived Gust Velocity per Nautical Mile, 4,500-9,500 Feet	A-59
Cumulative Occurrences of Derived Gust Velocity per Nautical Mile, 9,500-19,500 Feet	A-60
Cumulative Occurrences of Derived Gust Velocity per Nautical Mile, 19,500-29,500 Feet	A-61
Cumulative Occurrences of Derived Gust Velocity per Nautical Mile, 29,500-39,500 Feet	A-62
Cumulative Occurrences of Derived Gust Velocity per Nautical Mile, Flaps Extended	A-63
Cumulative Occurrences of Derived Gust Velocity per Nautical Mile, Flaps Retracted	A-64
<b>CONTINUOUS GUST INTENSITY DATA</b>	
Cumulative Occurrences of Continuous Gust Intensity per Nautical Mile, Flaps Extended	A-65
Cumulative Occurrences of Continuous Gust Intensity per Nautical Mile, Flaps Retracted	A-66
<b>GUST V-n DIAGRAM DATA</b>	
Gust Load Factor and Coincident Speed vs. V-n Diagram for Flaps Retracted	A-67
Gust Load Factor and Coincident Speed vs. V-n Diagram for Flaps Extended, Detents 10, 15, 20, and 40	A-68
<b>MANEUVER VERTICAL LOAD FACTOR DATA</b>	
Cumulative Occurrences of Incremental Vertical Maneuver Load Factor per 1000 Hours During Departure by Altitude	A-69
Cumulative Occurrences of Incremental Vertical Maneuver Load Factor per 1000 Hours During Climb by Altitude	A-70
Cumulative Occurrences of Incremental Vertical Maneuver Load Factor per 1000 Hours During Cruise by Altitude	A-71
Cumulative Occurrences of Incremental Vertical Maneuver Load Factor per 1000 Hours During Descent by Altitude	A-72
Cumulative Occurrences of Incremental Vertical Maneuver Load Factor per 1000 Hours During Approach by Altitude	A-73
Cumulative Occurrences of Incremental Vertical Maneuver Load Factor per Nautical Mile During Departure by Altitude	A-74
Cumulative Occurrences of Incremental Vertical Maneuver Load Factor per Nautical Mile During Climb by Altitude	A-75
Cumulative Occurrences of Incremental Vertical Maneuver Load Factor per Nautical Mile During Cruise by Altitude	A-76
Cumulative Occurrences of Incremental Vertical Maneuver Load Factor per Nautical Mile During Descent by Altitude	A-77
Cumulative Occurrences of Incremental Vertical Maneuver Load Factor per Nautical Mile During Approach by Altitude	A-78

Figures A-1 through A-118 are presented in appendix A. For ease of understanding, most of the figures in appendix A are presented in graphical form with a minimum of numerical summaries. In an effort to make the data presentation of a more comprehensive nature, some figures include both cumulative and relative probability or frequency distribution histograms as well as line plots. Scatter plots are also included where appropriate to show the relationship between coincident parameters that are considered to be of interest and to show visible evidence of relationships, outliers or suspicious data. The scatter plots presented in this report show that many of the plotted parameters are not related but occur in an independent random nature.

It should also be noted that the data presented in these figures are not always based on an identical number of flights or flight hours. During data reduction, it was discovered that some data frames and/or parameters exhibited random errors and were thus judged to be unacceptable for use. When this occurred, those "questionable data" were eliminated from the statistical database for any application, either directly or indirectly, of the other data measurements. As a result, not all figures are based on data from identical numbers of flights, hours, or nautical miles.

## 5.1 Aircraft Usage Data.

Figures A-1 through A-18 provide statistical data on the aircraft's operational usage. Information on takeoff and landing gross weights, operational flight speeds and altitudes, aircraft attitude, and flight lengths based on normal everyday flight operations are presented. These data are primarily useful in defining typical flight profiles including gross weight, speed, and altitude and the number of flights associated with each type profile.

### 5.1.1 Weight and Flight Distance Data.

This section presents statistical data on operational takeoff and landing gross weights, flight distances, and plots showing the correlation between weight and flight distance. The flight distances in these figures are based on the great circle distance (sometimes referred to as stage length) between departure and arrival points except for figure 4, which compares two methods of determining flight distance.

The cumulative probability distributions of gross weight during takeoff and landing are presented in figures A-1 and A-2. The occurrences of takeoff gross weight show a wide variation as one would expect due to differing fuel weights for different length flights and variable passenger and baggage loading. The landing weight distribution shows some tendency to group within a narrower range that could indicate use of fuel management that results in more consistent landing weights. However, the wide variations of both distributions could also result because some of the flights may not be refueled at each landing site. It is noteworthy that the maximum landing gross weight observed is very close to the maximum design landing gross weight of 142,195 lbs. listed in table 1.

Figure A-3 shows the cumulative probability distribution of the flight length from takeoff to landing for all A-320 flights. The distribution of flight length occurrences indicates that the flights tend to fall into three distinct groups. There is a grouping of short range flights of less

the middle to lower altitudes. These trends indicate a probable correlation between flight duration and the maximum altitude attained.

The cumulative probabilities of ground speed for taxi in and taxi out operations are presented in figure A-10. The taxi in speed is somewhat higher than the taxi out speed, which agrees with what has been observed with other aircraft models. This probably occurs because ground movement of inbound traffic to the terminal after landing is generally accomplished faster due to less traffic than movement from the terminal to the takeoff position with traffic present. It should be noted for this report that the taxi in phase of operation begins after the first turnoff from the active runway as compared to previous UDRI reports that included the runway turnoff speeds as part of the taxi in phase of operation. The higher taxi-in speeds, as observed in these earlier reports, probably occurred as the aircraft was exiting the runway during the turnoff.

Figures A-11 and A-12 show measured speeds plotted versus Mach number and airspeed limits,  $M_{MO}$  or  $V_{MO}$ , as defined in the aircraft flight manual. Each plotted point represents the airspeed or Mach number that yielded the greatest difference between the observed airspeed or Mach number and the speed or Mach number limit at its coincident altitude regardless of flight phase. For example, in one flight, the maximum speed, with respect to the limit, might have been attained in the climb phase, while in another flight the maximum speed may have occurred in a different phase. Also, it should be noted that the Mach number and airspeed points as plotted do not necessarily occur simultaneously.

While both plots indicate there are many flights that operate at speeds or Mach number values approaching or slightly exceeding the airspeed limits, the A-320 aircraft's onboard computers should only allow these speed limits to be exceeded for a few seconds before automatically responding to reduce the aircraft's speed to acceptable levels. UDRI checked a few of the points that are over the airspeed limit at the lower altitudes and they occurred for several seconds either during descent or near the end of the descent phase. Also, except for one flight, there is an obvious absence of points anywhere near the Mach or airspeed limits for those flights shown operating below 10,000 feet. The flight point occurring from this flight in both plots nearest the limit at 5,000 feet was checked and represented a valid data point for a normal flight. All of the other points shown as occurring below 10,000 feet were also investigated and resulted during flights of very short duration. The reason there were no points in these flights near the airspeed limits is probably because other speed restrictions such as those imposed for flap and/or landing gear operations further restrict the aircraft's airspeed at these altitudes and flight distances.

Figures A-13 and A-14 show the cumulative probabilities of calibrated airspeed at liftoff and at touchdown. Figure A-13 shows that the majority of takeoffs occur at speeds between 150 and 165 knots. Figure A-14 separates the landing speeds at touchdown for flights that were landed under manual control and those using the autoland system. About 1% of the total number of flights recorded were landed using the autoland system. Although most landing speeds at touchdown vary between 115 and 140 knots, the speeds associated with autolandings are slightly higher than those during manually controlled landings. Comparison of the two figures also shows that the liftoff speeds for the A-320 are approximately 30 knots higher than the touchdown speeds.

extent, the wing, fuselage, and empennage. (Statistical ground loads data for other aircraft models can be found in reference 2.)

### 5.2.1 Lateral Load Factor Data.

This section presents lateral load factor statistical data during aircraft ground turning operations and at touchdown.

Figure A-19 shows the cumulative occurrences of maximum lateral load factor that occur during ground turning operations (excludes the runway turnoff). The information is presented per 1000 flights for both preflight and postflight taxi and contains data for both left and right turns. The magnitudes of lateral load factor are about equal during taxi in and taxi out. Data for the B-737-400, MD-82/83, and B-767-200 aircraft, as reported in references 5, 6, and 7, showed that during taxi in, the lateral load factors are a little higher probably because of the higher speeds associated with taxi in. Also, figure A-19 shows no significant difference between the number of left and right turns or their magnitudes.

Figure A-20 presents the cumulative occurrences of maximum lateral load factor that occur per 1000 flights at touchdown. Because of the delay in the squat switch indication of touchdown and to ensure that the maximum  $n_y$  load factor peak associated with touchdown was identified, UDRI scanned an interval of 5 seconds prior to squat switch closure to identify the maximum  $n_y$  load factor peak during touchdown. The data show that  $n_y$  peaks during the landing touchdown fall between approximately  $-0.26$  to  $+0.3$  g's. The relative frequency distribution does not exhibit a distinguishable mode frequency but increases as the side load factor approaches zero from either direction. There were 565 flights that did not contain an  $n_y$  peak at touchdown, so the number of peaks does not equate to the number of flights.

Figure A-21 presents the occurrences of the maximum lateral load factor that occurred per 1000 flights during the first turnoff from the active runway after landing. This figure shows there were 3,551 flights that turned right and 6,515 flights that turned left off the runway, which is more of a disparity than one would expect, but is a function of the airport/runway layout and traffic patterns. However, the magnitude of lateral load factor between about  $\pm 0.3$  g's for right and left turns is very similar, as one would expect. These lateral load factor occurrences are not included in the taxi in data presented in figure 19. Thus, when figures 19 and 21 are compared, it can be seen that values of lateral load factor are slightly higher during runway turnoff.

Figure A-22 presents the coincident incremental vertical load factor that occurs in conjunction with the maximum lateral load factor at touchdown (the same 5-second interval as defined above was used to identify touchdown). Some of the flights did not experience an  $n_y$  peak associated with touchdown; therefore, no coincident  $n_z$  values were plotted for these flights. The data show that the highest vertical load factor peaks occur in conjunction with the lower magnitude occurrences of lateral load factor. Similarly, when the highest lateral load factors occur, the vertical load factors tend to be at the lower end of their range.

Figure A-23 shows the probability of the turn angle (total angular measurement) experienced during 10,066 turnoffs from the active runway. The plot indicates that a significant number of turns are grouped around 30, 90, and 180 degrees. Then, the scatter plots, figures A-24 through

of attack during liftoff for various selected speed ranges; and the aircraft's acceleration response due to operations on runways within this operator's system.

Figure A-33 presents cumulative occurrences of incremental vertical load factor per 1000 flights for the taxi in and taxi out phases of ground operations. The data show that the distribution of vertical load factor during taxi-in is slightly higher than for taxi out. This slight difference was also observed on the B-737-400, MD-82/83, and B-767 aircraft [5, 6, 7] and is probably due to the slightly higher taxi in speeds shown in figure A-10.

Figure A-34 presents the cumulative occurrences of positive and negative incremental vertical load factors per 1000 flights that occurred during the takeoff roll. While the magnitudes of load factor appear to be consistent with what one would expect during the takeoff roll, these values are primarily a function of the condition or "roughness" of the runway.

Figure A-35 presents the cumulative occurrences of the minimum and maximum incremental vertical load factor per 1000 flights associated with touchdown and deployment of the ground spoilers. This figure shows that approximately the same minimum and maximum load factor peaks,  $-0.5\text{ g}$  and  $+1.0\text{ g}$ , respectively, are attributable to each event. These identical readings probably occur because the sampling rate for each event indicator is only once per second and deployment of the ground spoilers occurs very quickly after touchdown. Thus, when this occurred, it was impossible to determine which event actually caused the minimum and maximum load factor peaks. So, unless the peaks were separated by several seconds, the same minimum or maximum peak was probably identified and assigned as having occurred both at touchdown and during deployment of the spoilers.

Figure A-36 presents the cumulative occurrences of incremental vertical load factor per 1000 flights during the landing roll for operations with and without thrust reversers. These curves may also include the effects of ground spoiler usage on vertical load factor because the spoilers are normally used during the landing rollout concurrently with the thrust reversers.

Figures A-37 through A-42 contain scatter plots that show the maximum incremental vertical load factor versus the maximum angle of attack attained within a 10-second interval after liftoff and the coincident airspeed/range at which they occurred. While the plots show that the maximum angle of attack during liftoff tends to decrease with increasing airspeed, there doesn't appear to be any correlation between angle of attack and vertical acceleration. The airspeed ranges of 150-160 knots in figures A-39 and 160-179 knots in figure A-40 generate the largest number of acceleration peaks because they are the speeds most frequently used during liftoff.

Figures A-43 through A-47 contain scatter plots that show the maximum incremental vertical load factor at touchdown versus the yaw angle, bank angle, wind speed, and inertial vertical velocity before touchdown. The values of yaw angle, bank angle, and wind speed values used here are the same as those derived and used previously in figures A-27 through A-30. The values of mean inertial vertical velocity contained in figure A-47 were obtained by averaging the recorded values between  $-50$  seconds and  $-10$  seconds prior to aircraft touchdown. The final 10 seconds of flight data were not used because of concerns about the accuracy of these measurements due to ground effects.

incremental vertical gust load factor encountered by the A-320 was 1.0 g and occurred, as shown in Figure A-50, during the approach phase of flight.

Figure A-52 presents the cumulative occurrences of incremental vertical gust load factor per nautical mile by phase of flight, and figure A-53 shows the cumulative occurrences of incremental vertical gust load factor for all the airborne phases combined per nautical mile.

### 5.3.2 Derived Gust Velocity Data.

The magnitudes for the gust velocities were derived from the measured accelerations in accordance with the procedures presented in section 4.2.4. In figures A-54 and A-55, derived gust velocity,  $U_{de}$ , is plotted as cumulative occurrences per nautical mile for altitudes above the airport; in figures A-56 through A-62,  $U_{de}$ , is plotted as cumulative occurrences per nautical mile for pressure altitudes from sea level to 39,500 feet. In each figure, the derived gust velocities are compared to the gust velocity distributions presented in reference 8, which is an established standard that is often used in establishing structural design criteria for repeated gust loads.

Figures A-63 and A-64 present derived gust velocity,  $U_{de}$ , per nautical mile for the flaps extended and retracted conditions, respectively.

### 5.3.3 Continuous Gust Intensity Data.

The magnitudes of the continuous gust intensities,  $U_o$ , were derived from the measured accelerations in accordance with the procedures presented in section 4.2.5. The cumulative occurrences of continuous gust intensity per nautical mile for the flaps extended and retracted conditions are presented in figures A-65 and A-66, respectively.

### 5.3.4 Gust V-n Diagram Data.

Federal Aviation Regulation (FAR) 25.333 requires that strength requirements be met at each combination of airspeed and load factor on and within the boundaries of the representative gust load envelopes (V-n diagrams). For the gust V-n diagram, the required limit load factors for gusts result from gust velocities as specified in FAR 25.341. The FAR specifies positive (up) and negative (down) air gust design requirements for three different aircraft design speeds: maximum gust intensity speed ( $V_B$ ), cruising speed ( $V_C$ ), and dive speed ( $V_D$ ).

To display the coincident speed and gust accelerations, representative V-n diagrams were developed for the flaps retracted and extended configurations for illustration purposes only. Since V-n diagrams are a function of altitude and gross weight, the maximum takeoff gross weight of 162,083 pounds for the flaps retracted configuration and a landing gross weight of 130,000 pounds for the flaps extended configuration were selected at an altitude of sea level. The landing gross weight was selected as representing a median value based on the data as shown in figure A-2.

Figures A-67 and A-68 show the coincident gust acceleration and airspeed measurements plotted on the V-n diagrams for the flaps retracted and extended configurations, respectively. All flap

factor is 2.0 g when the flaps are extended. Maneuver strength is required for three different aircraft design speeds: flaps down speed ( $V_F$ ), cruising speed ( $V_C$ ), and dive speed ( $V_D$ ). As with the V-n diagram for gust loads, the maximum takeoff gross weight of 162,083 pounds for the flaps retracted configuration and the maximum landing gross weight of 130,000 pounds for the flaps extended configuration were selected to develop representative maneuver V-n diagrams.

Figures A-83 and A-84 show the maneuver V-n diagrams with flaps retracted and extended with the coincident acceleration and speed measurements. All flap detent positions for which data were available (10, 15, 20, and 40), are shown in figure A-84 to provide a range of flap extension conditions. Figure A-84 shows, for the flaps extended cases, that a few maneuver acceleration points occur at speeds outside the maneuver V-n diagram. These results are similar to those observed on other aircraft [5, 6, 7] with the flaps extended.

### 5.3.7 Combined Maneuver and Gust Vertical Load Factor Data.

Figure A-85 shows the cumulative occurrences of the combined maneuver and gust incremental vertical load factor per 1000 hours by phases of flight, and figure A-86 shows the incremental vertical load factor occurrences for all flight phases combined.

Figures A-87 and A-88 contain the same vertical load factor data as figures A-85 and A-86 but are plotted as occurrences per nautical mile by phases of flight and for all flight phases combined. The 1-g incremental gust load factor encountered during the approach phase of flight is still the highest load factor recorded for the A-320's operation.

### 5.3.8 Combined Maneuver and Gust Lateral Load Factor Data.

Figure 89 presents the cumulative occurrences of lateral load factor per 1000 hours by phase of flight. Maximum lateral load factor values between approximately -0.32 and +0.19 g's were observed during flight operations of the A-320.

Figures A-90 through A-94 contain scatter plots that show the maximum lateral load factor versus the coincident gross weight of the aircraft during the airborne phases of flight.

### 5.3.9 Ground-Air-Ground Cycle Data.

Figures A-95 and A-96 display occurrences of the maximum and minimum incremental vertical load factor that occurs once per flight. The load excursion between the largest negative and highest positive load factor is often referred to by aircraft design engineers as the Ground-Air-Ground or GAG cycle. Figure A-95 presents the number of GAG cycle occurrences in tabular form and figure A-96 shows the number of GAG cycle occurrences plotted as a three-dimensional (3-D) bar chart. The GAG cycle usually contributes the most damaging fatigue cycle experienced by the aircraft wing and carry through structural assemblies. The GAG cycle that contained the widest range between negative and positive occurred between -0.95 and +0.65 g's.

### 5.4.3 Landing Gear Data.

Statistical data showing the speeds, altitudes, and vertical load factor when the landing gear is started to be retracted or extended are shown in figures A-108 through A-113. This information characterizes the operational usage of the landing gear for the airline and also provides data for the aircraft manufacturer that can be used to assess the loading conditions for the landing gear and backup structure.

Figures A-108 and A-109 contain scatter plots showing the coincident speed and altitude above the airport at the start of gear retraction and extension. Although figure A-108 shows considerable scatter, the beginning of the landing gear retraction cycle most often occurs around 160 knots and about 700 feet in altitude above the airport. While figure A-109 also shows a lot of scatter between speed and altitude when the landing gear extension cycle begins, the landing gear extension appears to occur most often between 160-190 knots at altitudes ranging from around 1000 feet up to about 3000 feet.

Figures A-110 and A-111 contain the same data points used to generate the scatter plots shown in figures A-108 and A-109 but are plotted here as the probability of speed and altitude above the airport at the beginning of landing gear extension and retraction.

Figures A-112 and A-113 contain scatter plots that show the maximum and minimum incremental vertical load factor versus coincident airspeed at the beginning of landing gear extension and retraction.

### 5.4.4 Thrust Reverser Data.

The times and speeds associated with thrust reverser operations were derived from the measured data. Figure A-114 presents the cumulative probability of time during which the thrust reversers are deployed. The data show that for 90 percent of the flights the thrust reversers are deployed for less than 25 seconds. Figure A-115 presents the cumulative probability of the speed at the time the thrust reversers were deployed and stowed. Most thrust reverser deployment cycles begin at speeds between 100 and 120 knots and are stowed at speeds between 40 and 80 knots.

### 5.4.5 Brake Application Data.

The time from aircraft touchdown to initial application of the brakes and the time duration for which braking occurred during the landing roll are presented. Figure A-116 shows the probability of time to application of the brakes after touchdown. The most frequent time to initial brake application ranges from about 10 to 30 seconds. Figure A-117 shows the probability of the duration of brake application during the landing roll after landing. The duration of braking that occurs the most often lasts from about 5 to 30 seconds.

### 5.4.6 Propulsion Data.

Figure A-118 presents the cumulative probability of the maximum engine fan speed  $N_1$  during takeoff, at the instant of thrust reverser deployment during the landing roll, and during the time that the thrust reverser is deployed. Most takeoffs occur at fan speed values ranging between

3. Rustenburg, John W., Donald A. Skinn, and Daniel O. Tipps, "An Evaluation of Methods to Separate Maneuver and Gust Load Factors from Measured Acceleration Time Histories," DOT/FAA/AR-99/14, April 1999.
4. Chai, Sonny T. and William H. Mason, "Landing Gear Integration in Aircraft Conceptual Design," Virginia Polytechnic Institute and State University Report MAD 96-09-01, September 1996 (rev. March 1997).
5. "Flight Loads Data for a Boeing 737-400 in Commercial Operation," FAA Report DOT/FAA/AR-98/28, August 1998.
6. "Flight Loads Data for a MD-82/83 in Commercial Operation," FAA Report DOT/FAA/AR-98/65, February 1999.
7. "Statistical Loads Data for B-767-200 Aircraft in Commercial Operation," FAA Report DOT/FAA/AR-00/10, March 2000.
8. Press, Harry and Roy Steiner, "An Approach to the Problem of Estimating Severe and Repeated Gust Loads for Missile Operations," National Advisory Committee for Aeronautics Technical Note 4332, Langley Aeronautical Laboratory, Langley Field, Va., September 1958.

APPENDIX A—DATA PRESENTATION

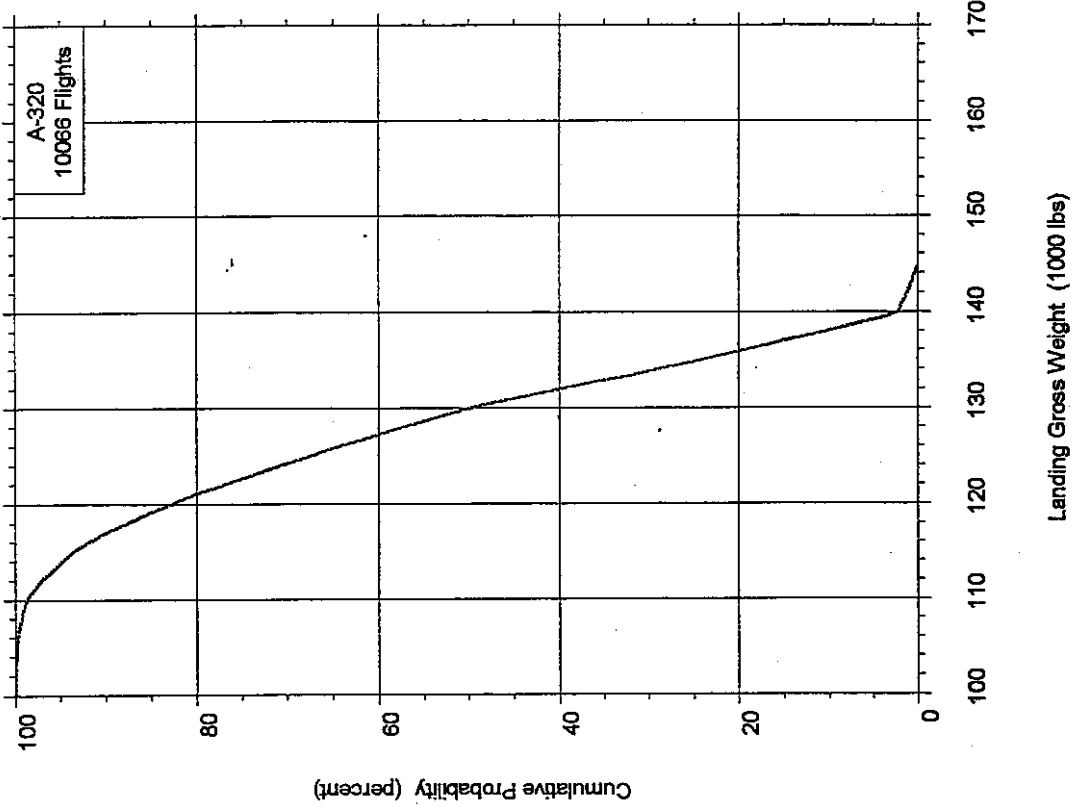


FIGURE A-1. CUMULATIVE PROBABILITY OF TAKEOFF GROSS WEIGHT

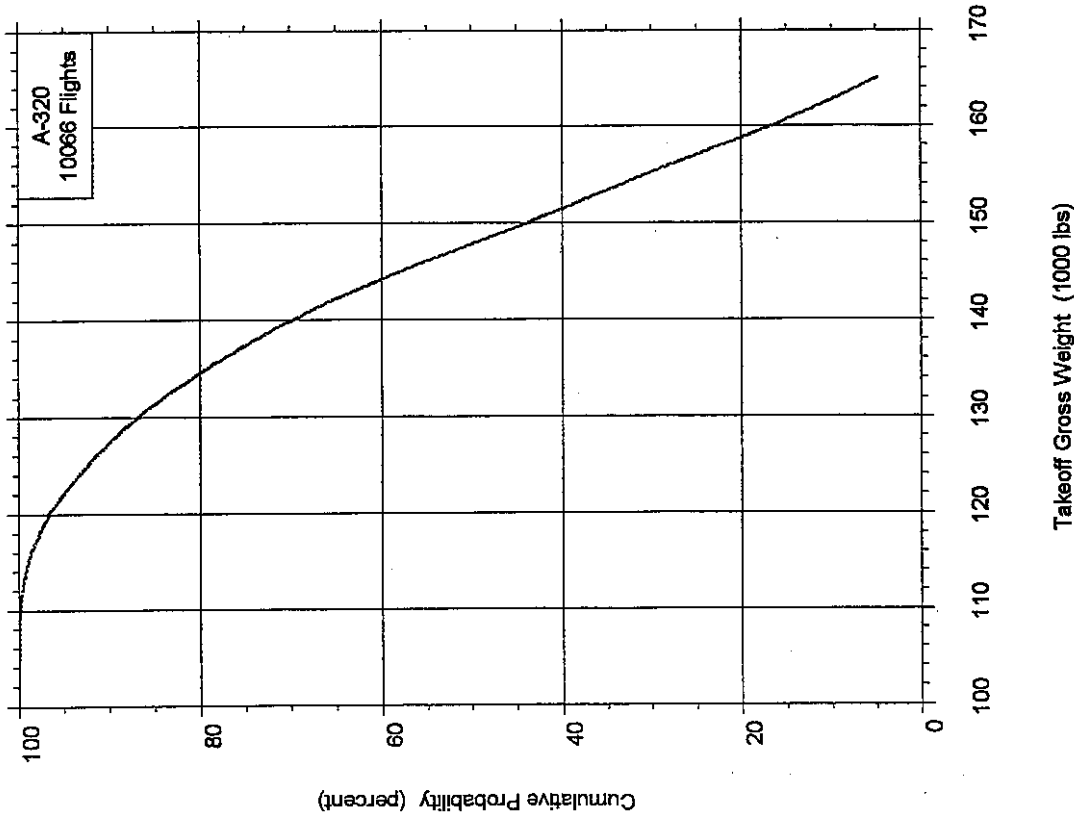


FIGURE A-2. CUMULATIVE PROBABILITY OF LANDING GROSS WEIGHT

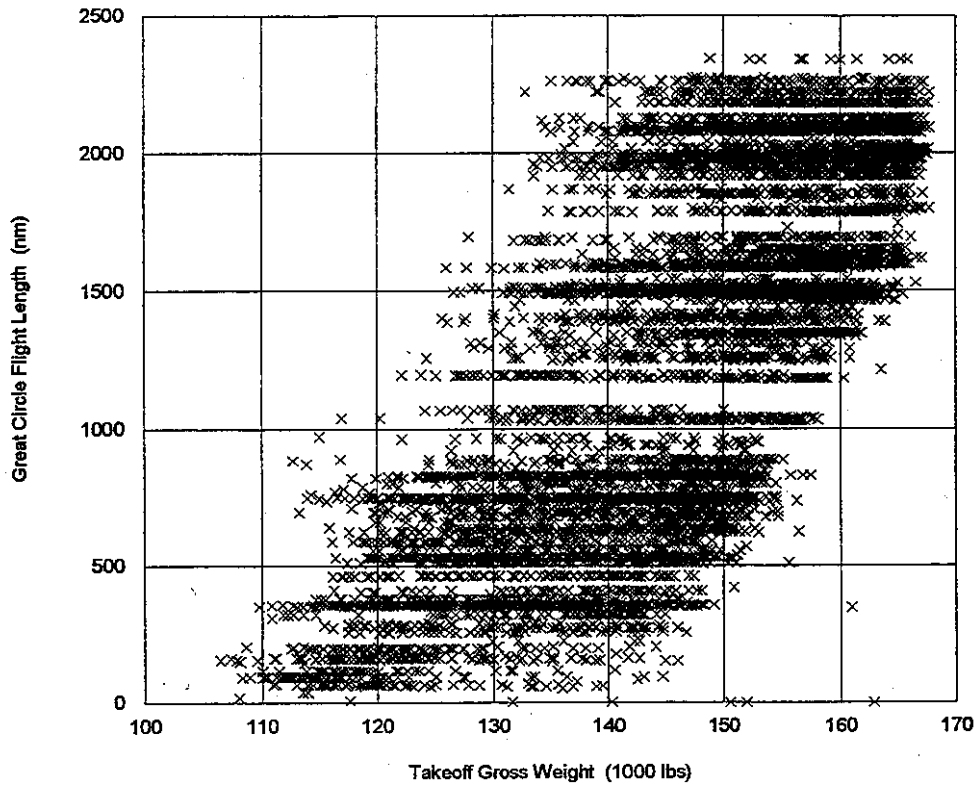


FIGURE A-5. CORRELATION OF TAKEOFF GROSS WEIGHT AND GREAT CIRCLE FLIGHT LENGTH

Takeoff Gross Weight (1000 lbs)

10000 Flts	100-110	110-120	120-130	130-140	140-150	150-160	160-170	Total
0-250	0.089	1.838	1.321	0.487	0.139	0.020	0.010	3.904
250-500	0.010	0.864	2.752	3.924	2.086	0.010	0.010	9.656
500-750		0.368	4.371	6.338	7.510	0.825		19.412
750-1000		0.139	0.944	2.424	4.947	1.371		9.825
1000-1250		0.010	0.228	1.033	1.212	1.431	0.020	3.934
1250-1500			0.109	1.202	2.861	6.666	1.331	12.170
1500-1750			0.070	0.874	2.503	6.030	2.643	12.120
1750-2000				0.437	2.444	4.729	5.037	12.647
2000-2250				0.209	2.027	5.722	7.252	15.210
2250-2500				0.099	0.278	0.457	0.288	1.123
Total	0.099	3.219	9.795	17.028	26.008	27.260	16.591	100.000

Great Circle Flight Length (nm)

FIGURE A-6. CORRELATION OF TAKEOFF GROSS WEIGHT AND GREAT CIRCLE FLIGHT LENGTH, PERCENT OF FLIGHTS

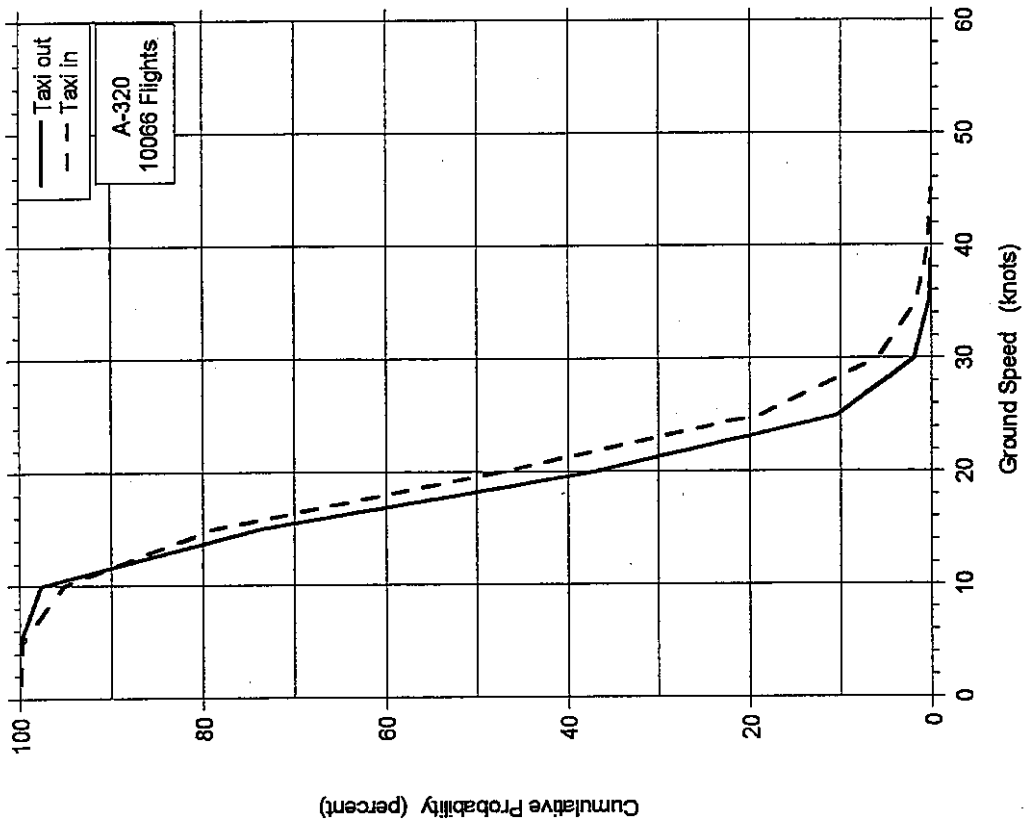


FIGURE A-10. CUMULATIVE PROBABILITY OF  
MAXIMUM GROUND SPEED DURING TAXI

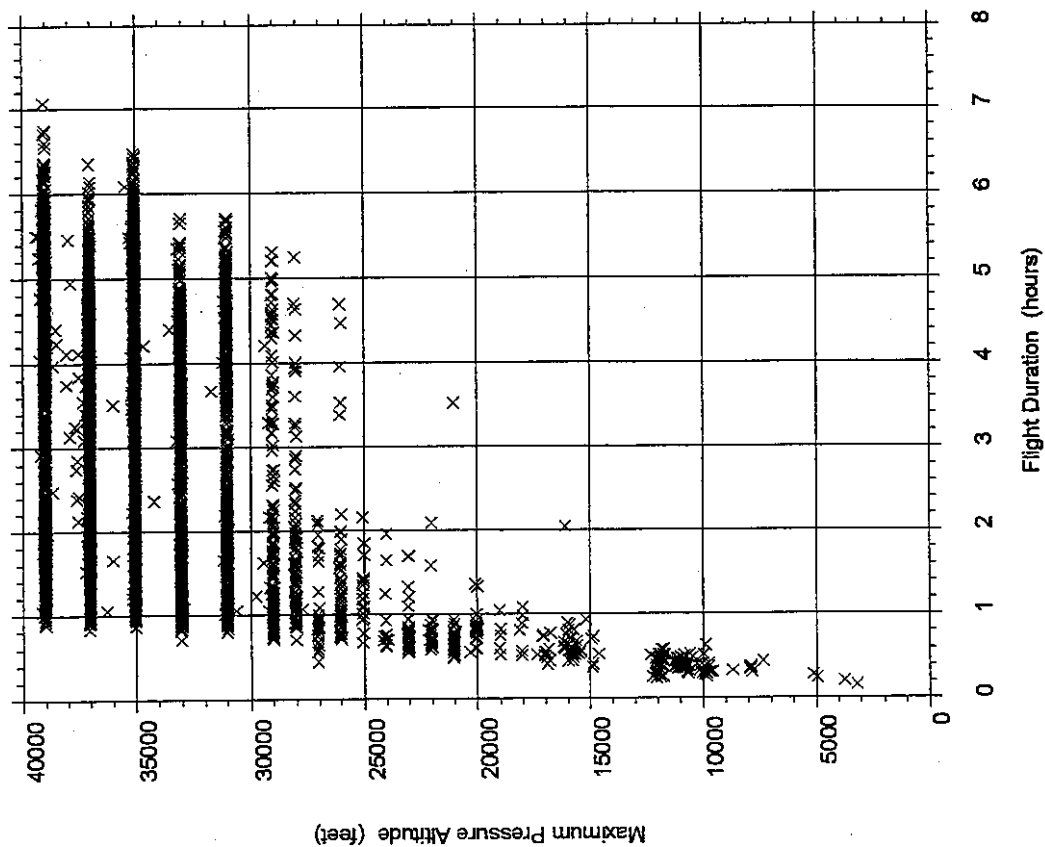


FIGURE A-9. CORRELATION OF MAXIMUM ALTITUDE  
AND FLIGHT DURATION

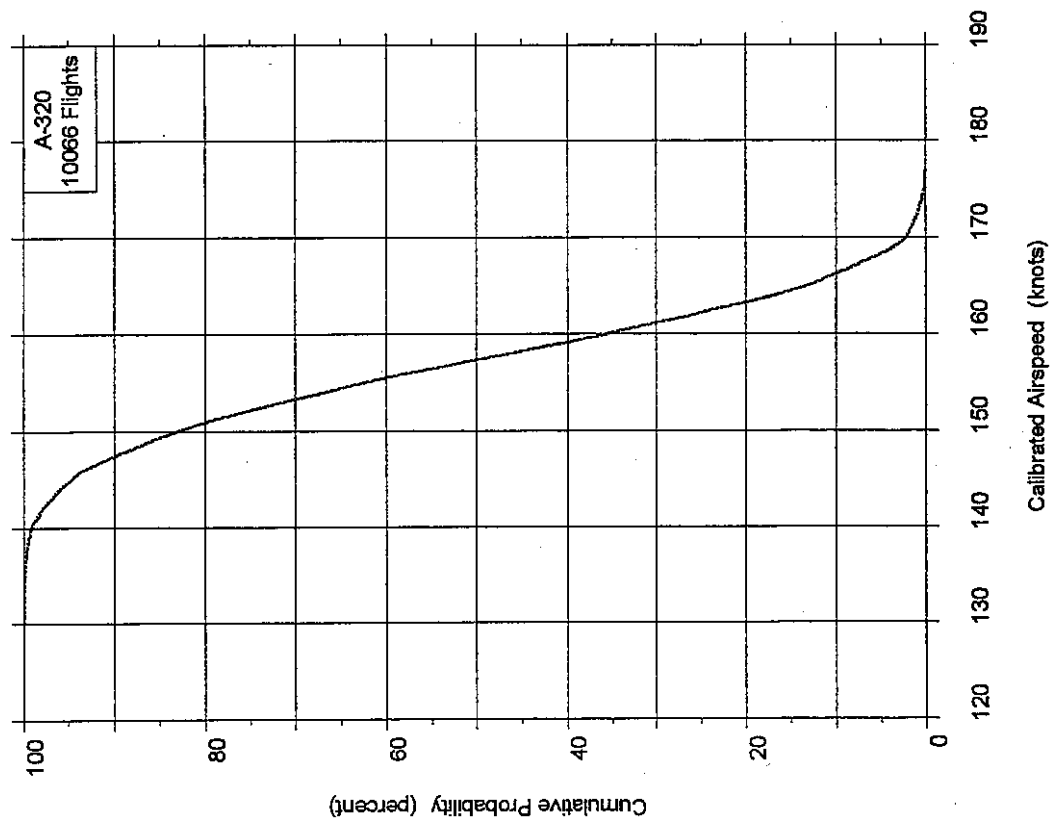


FIGURE A-13. CUMULATIVE PROBABILITY OF AIRSPEED AT LIFTOFF

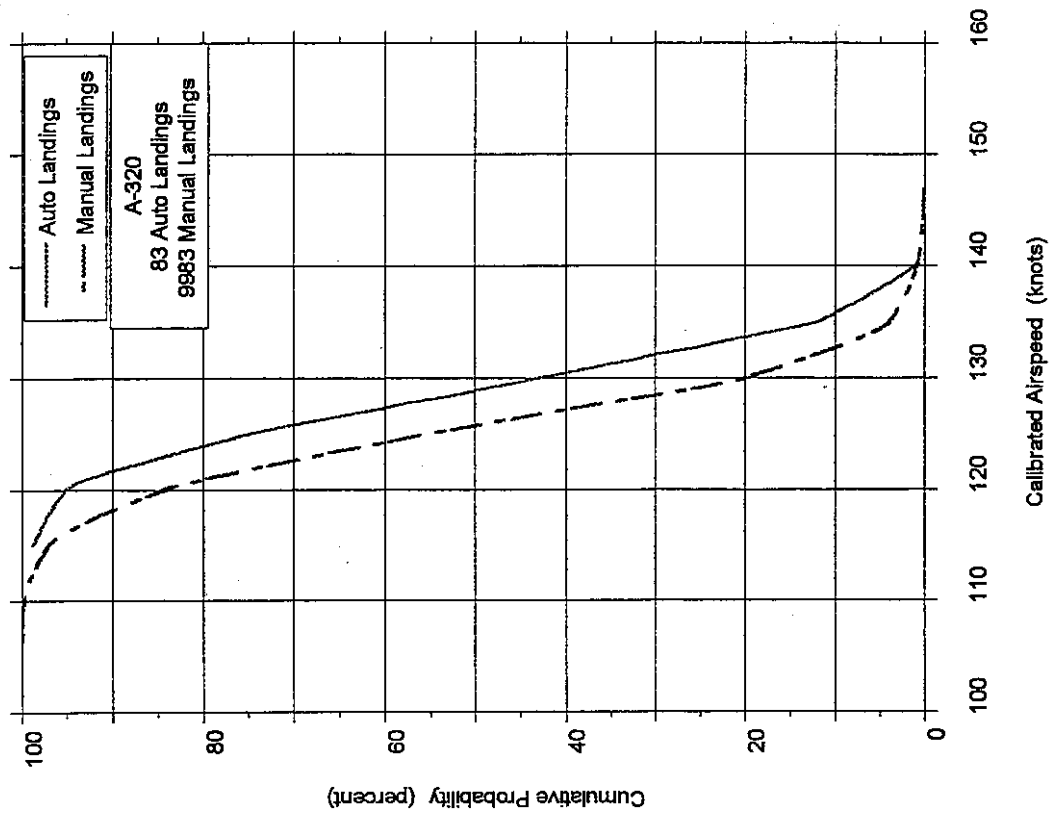


FIGURE A-14. CUMULATIVE PROBABILITY OF AIRSPEED AT TOUCHDOWN

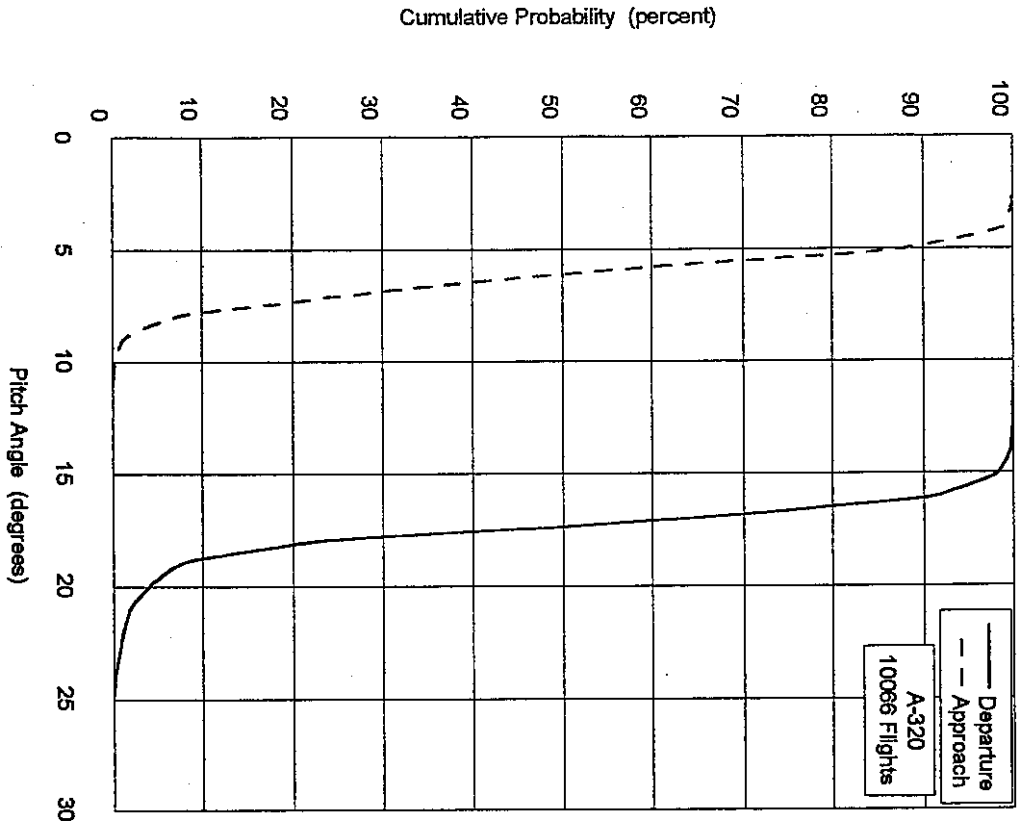


FIGURE A-17. CUMULATIVE PROBABILITY OF MAXIMUM PITCH ANGLE DURING DEPARTURE AND APPROACH

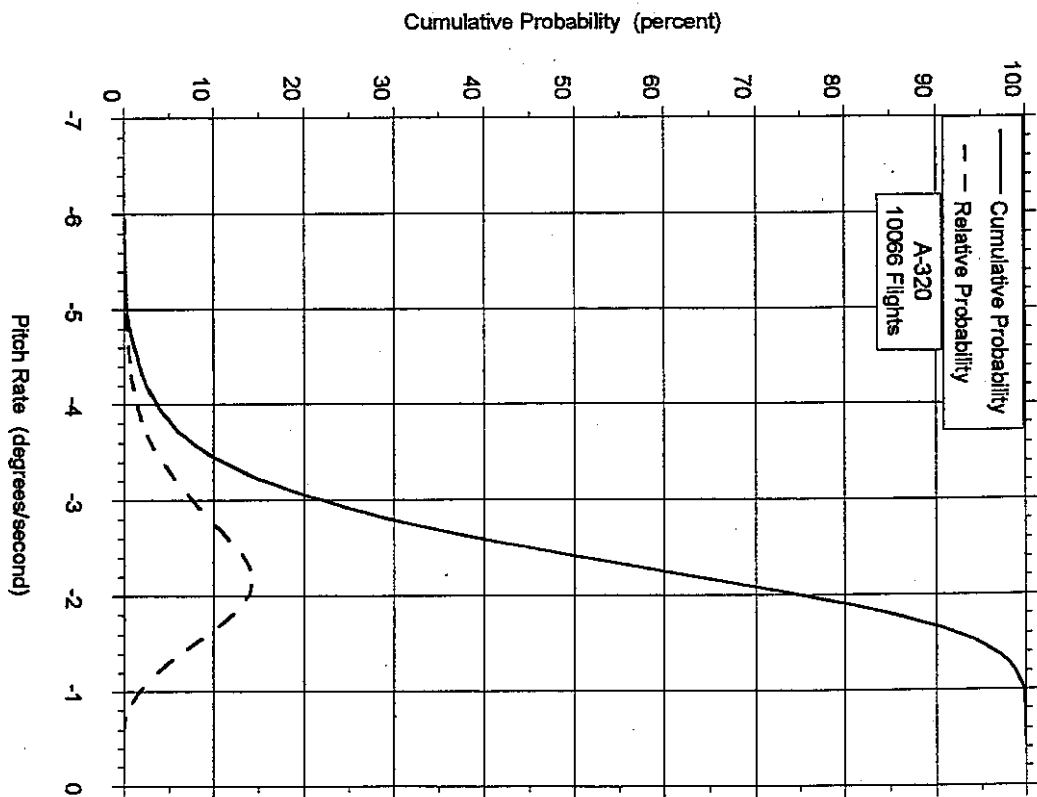


FIGURE A-18. PROBABILITY DISTRIBUTIONS OF MAXIMUM PITCH RATE AT NOSE GEAR TOUCHDOWN

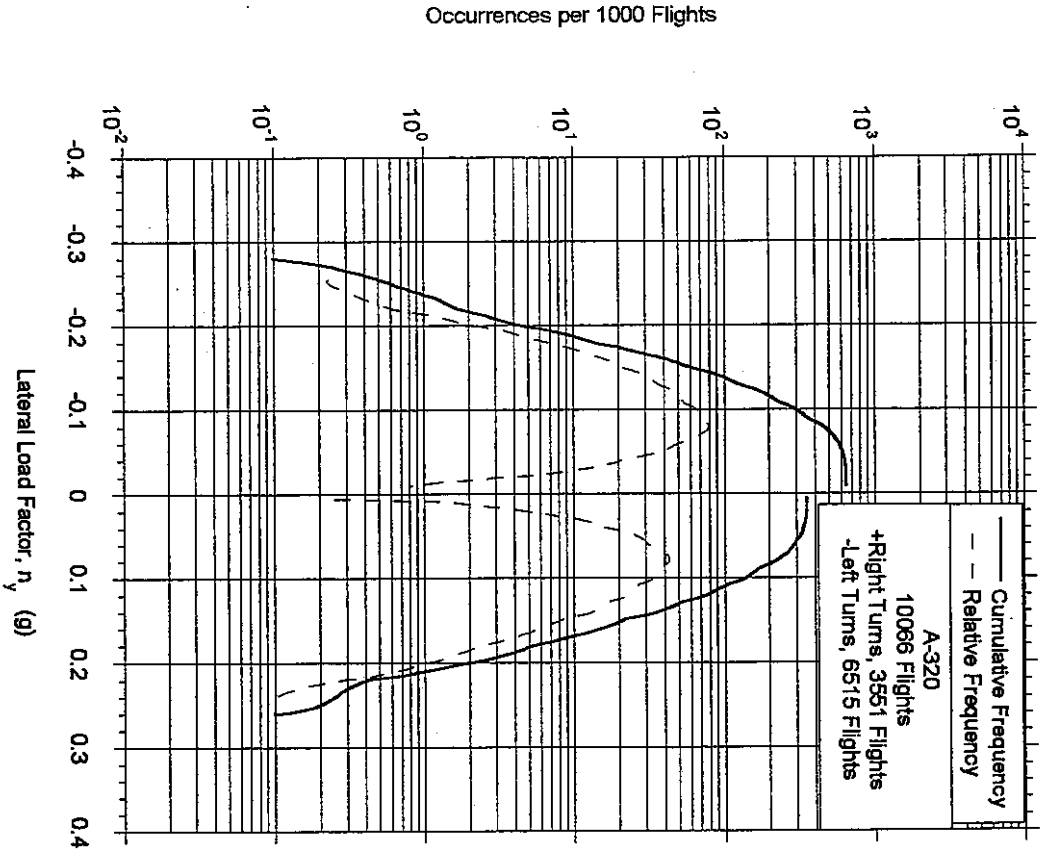


FIGURE A-21. FREQUENCY DISTRIBUTIONS OF MAXIMUM LATERAL LOAD FACTOR DURING RUNWAY TURNOFF

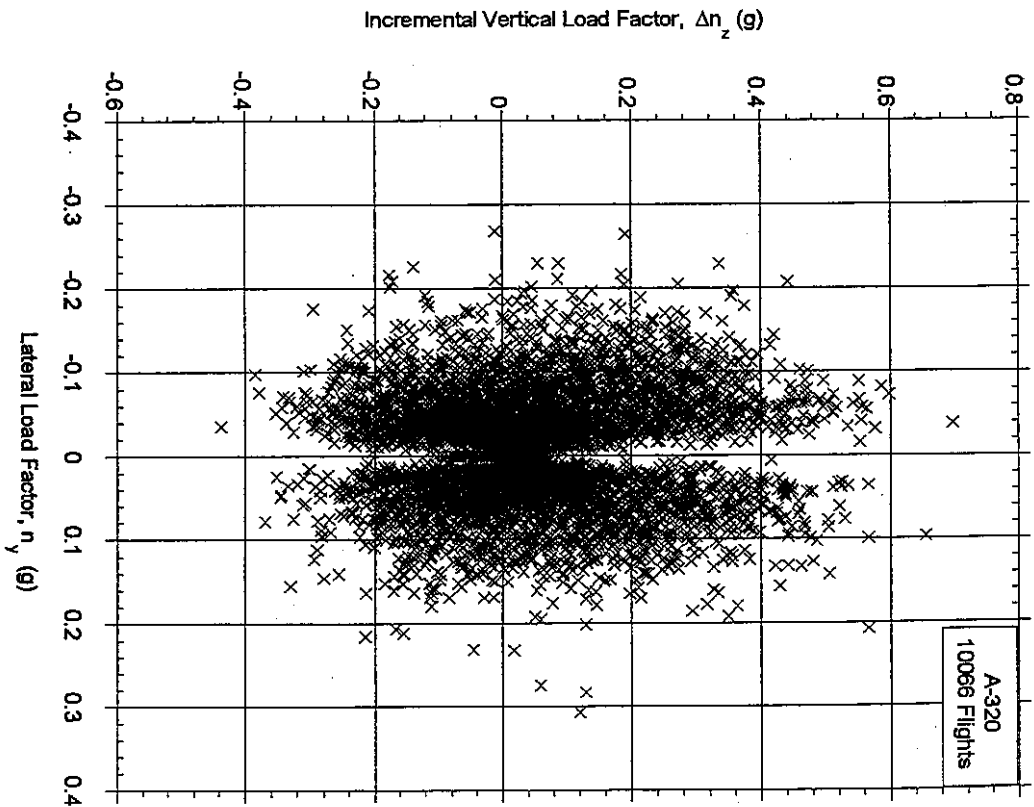


FIGURE A-22. MAXIMUM LATERAL LOAD FACTOR AND COINCIDENT INCREMENTAL VERTICAL LOAD FACTOR AT TOUCHDOWN

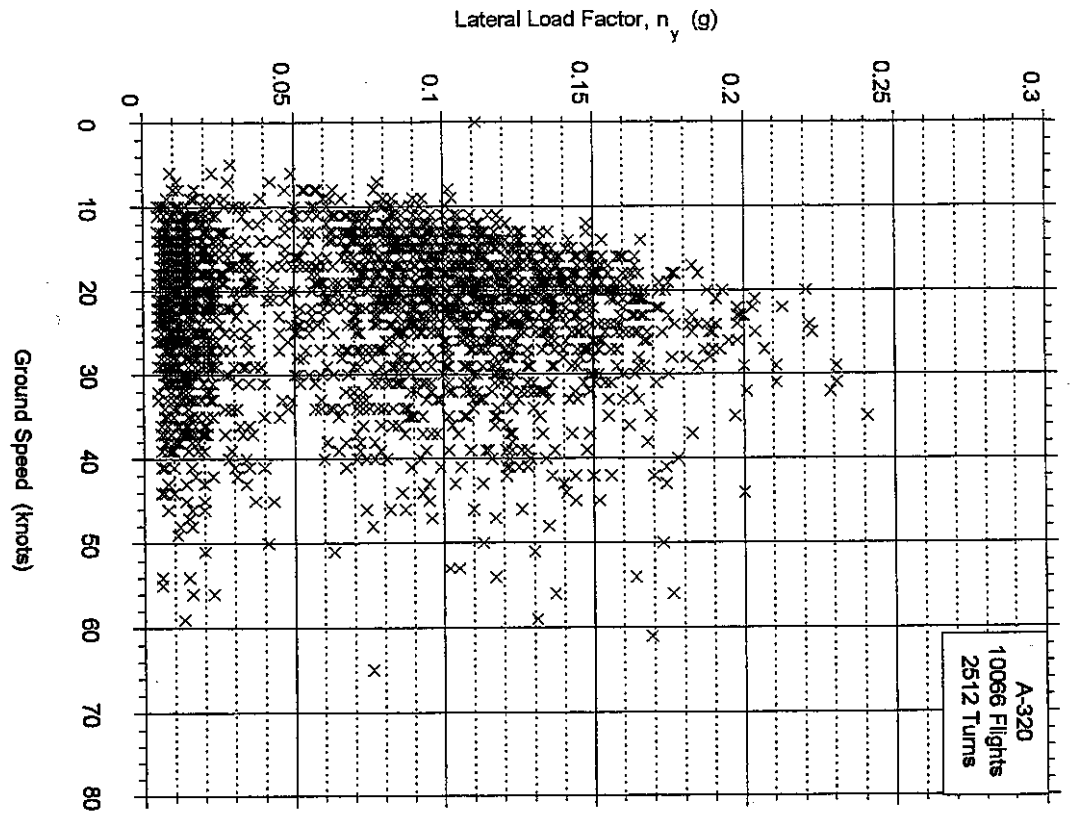


FIGURE A-25. MAXIMUM LATERAL LOAD FACTOR AND  
COINCIDENT GROUND SPEED DURING RUNWAY  
TURNOFF, 60-120 DEGREE TURNS

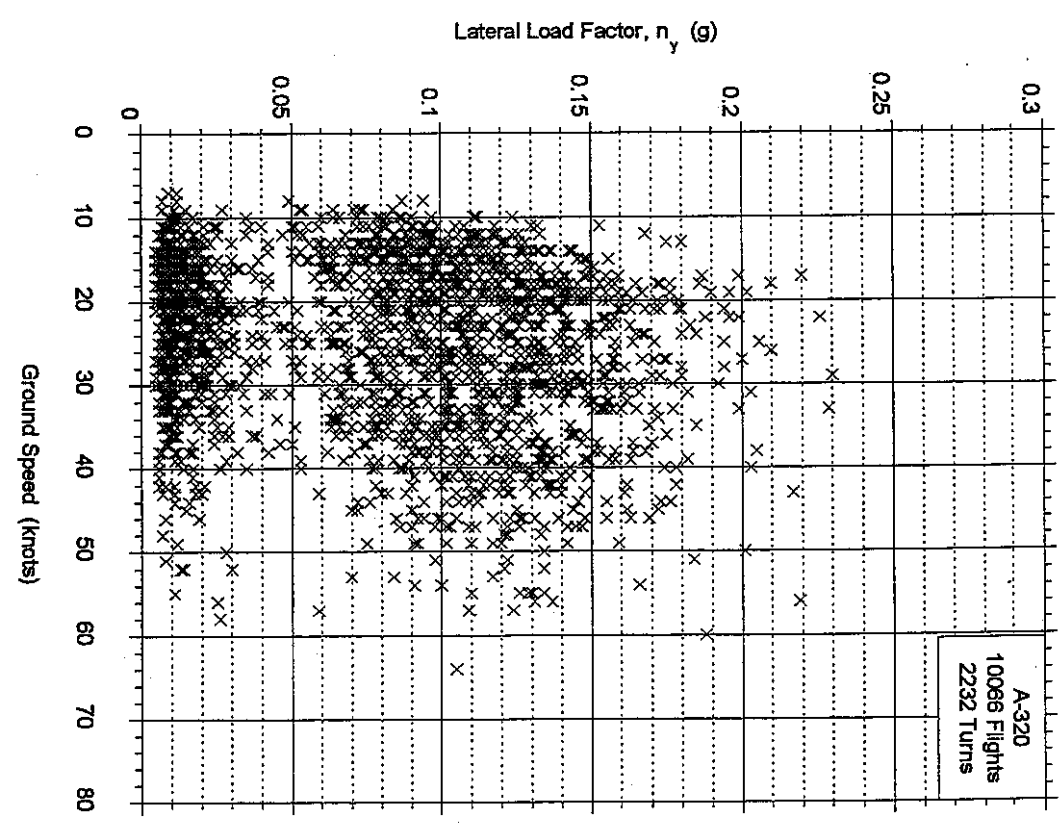


FIGURE A-26. MAXIMUM LATERAL LOAD FACTOR AND  
COINCIDENT GROUND SPEED DURING RUNWAY  
TURNOFF, 120-240 DEGREE TURNS

FIGURE A-30. MAXIMUM LATERAL LOAD FACTOR AT TOUCHDOWN VS. MEAN WIND SPEED BEFORE TOUCHDOWN

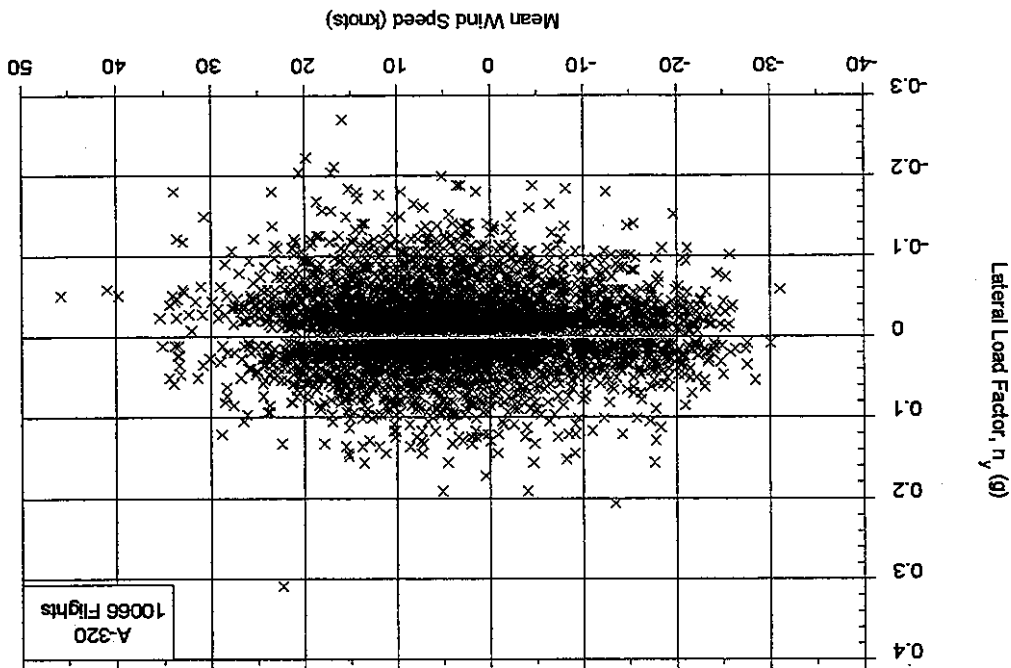
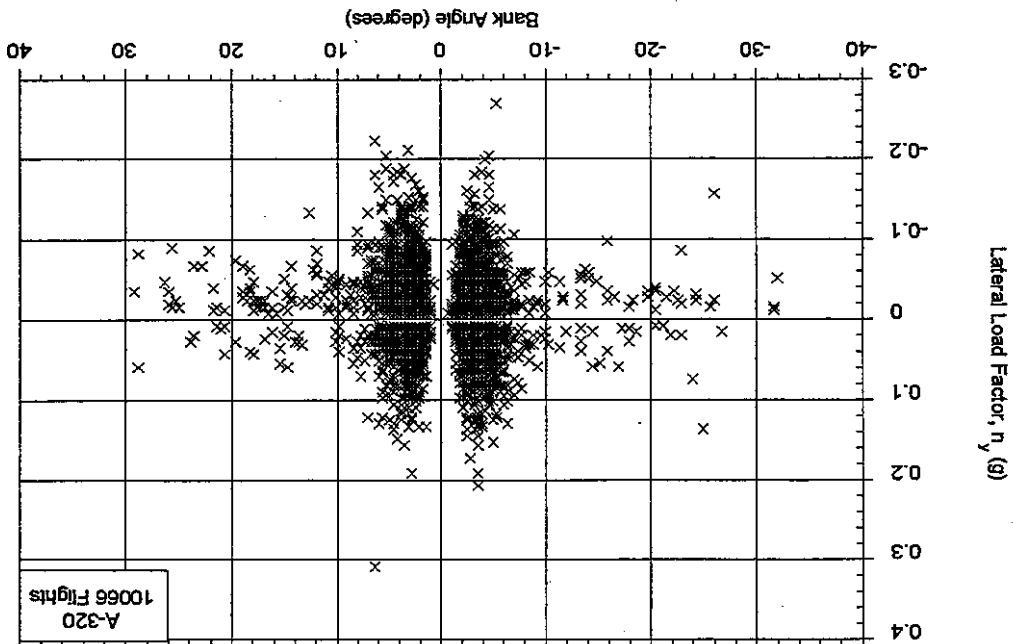


FIGURE A-29. MAXIMUM LATERAL LOAD FACTOR AT TOUCHDOWN VS. MAXIMUM BANK ANGLE BEFORE TOUCHDOWN



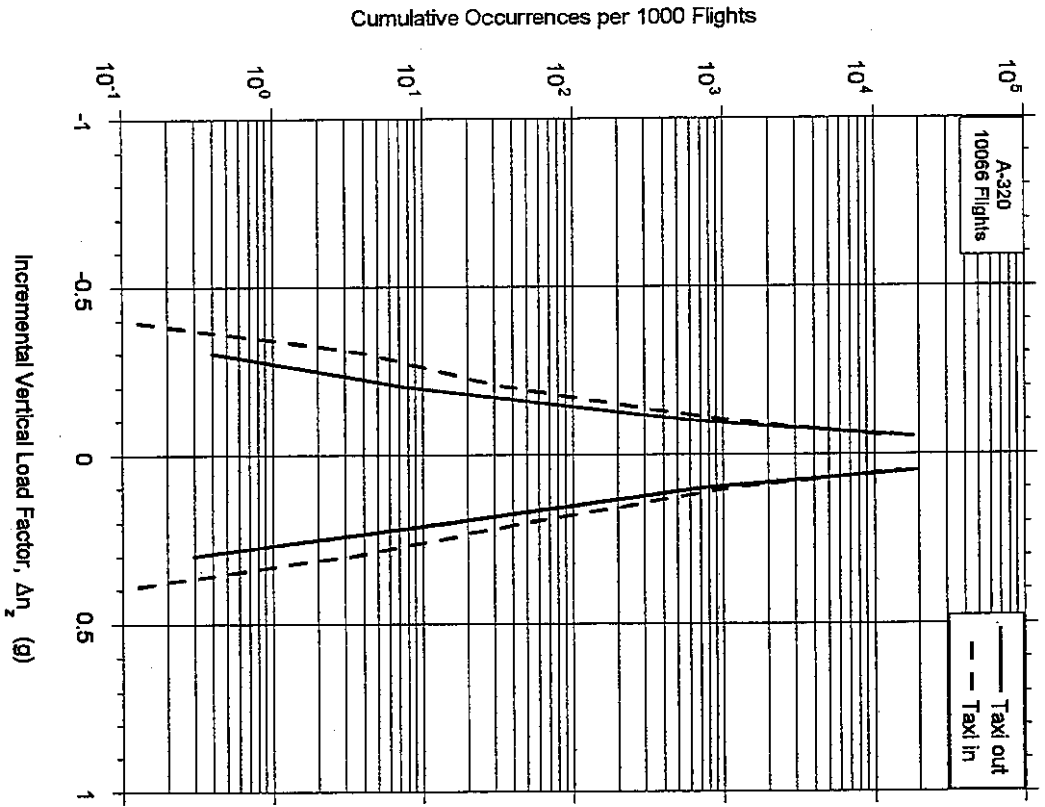


FIGURE A-33. CUMULATIVE FREQUENCY OF INCREMENTAL VERTICAL LOAD FACTOR DURING TAXI OPERATIONS

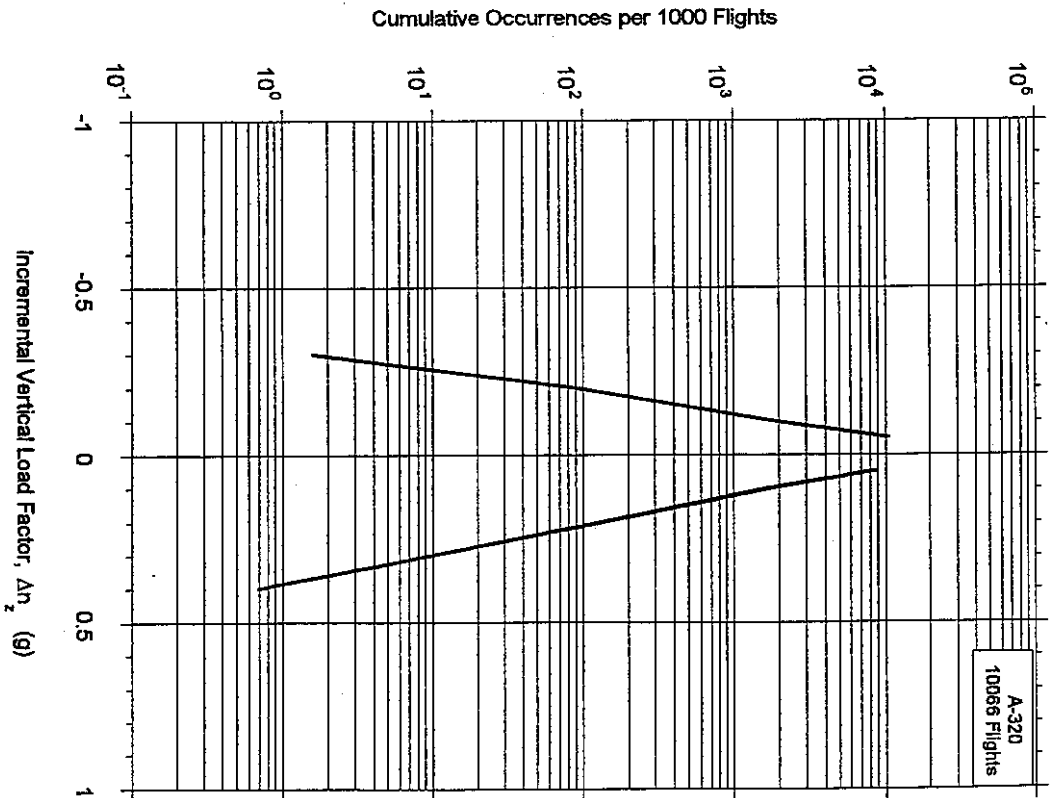


FIGURE A-34. CUMULATIVE FREQUENCY OF INCREMENTAL VERTICAL LOAD FACTOR DURING TAKEOFF ROLL

FIGURE A-38. MAXIMUM INCREMENTAL VERTICAL LOAD FACTOR VS. MAXIMUM ANGLE OF ATTACK DURING LIFTOFF, 140-150 KNOTS

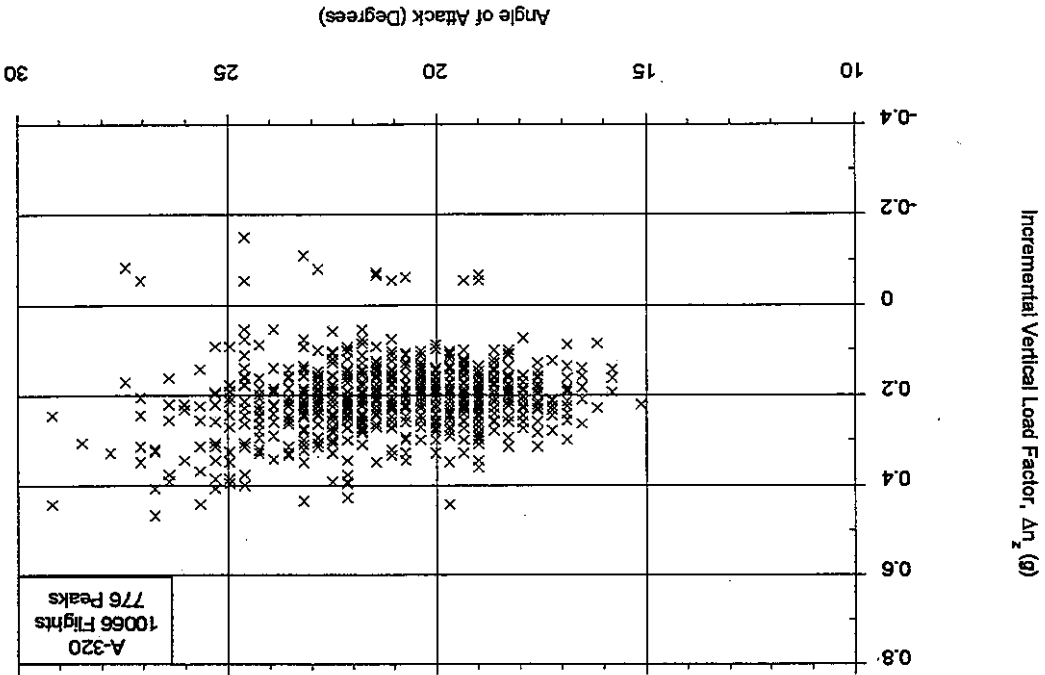


FIGURE A-37. MAXIMUM INCREMENTAL VERTICAL LOAD FACTOR VS. MAXIMUM ANGLE OF ATTACK DURING LIFTOFF, 130-140 KNOTS

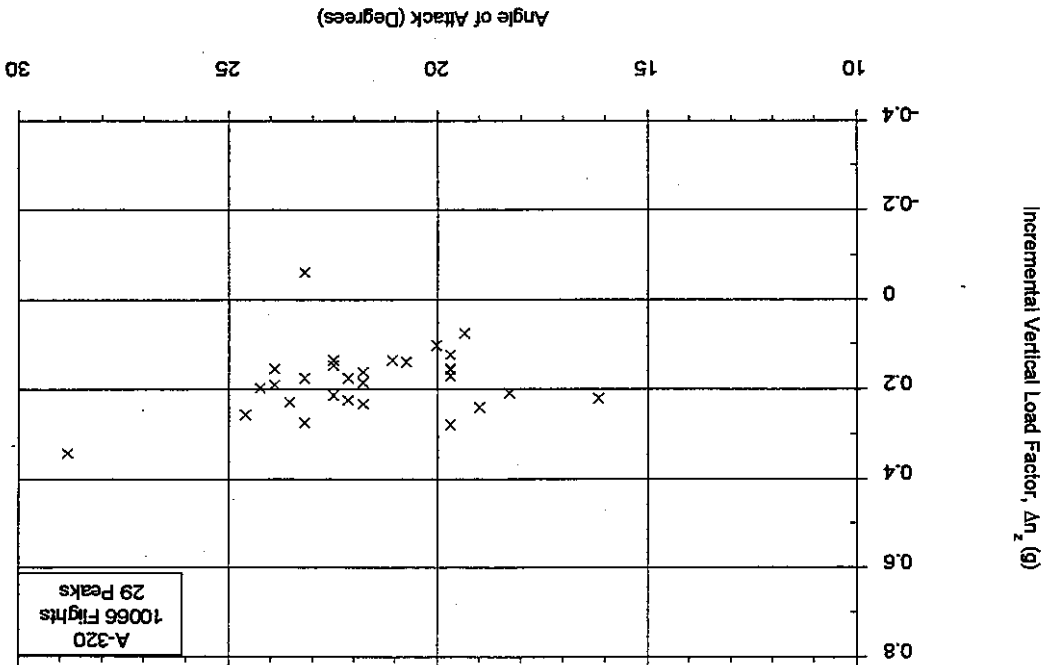


FIGURE A-42. MAXIMUM INCREMENTAL VERTICAL LOAD FACTOR VS. MAXIMUM ANGLE OF ATTACK DURING LIFTOFF, 180-190 KNOTS

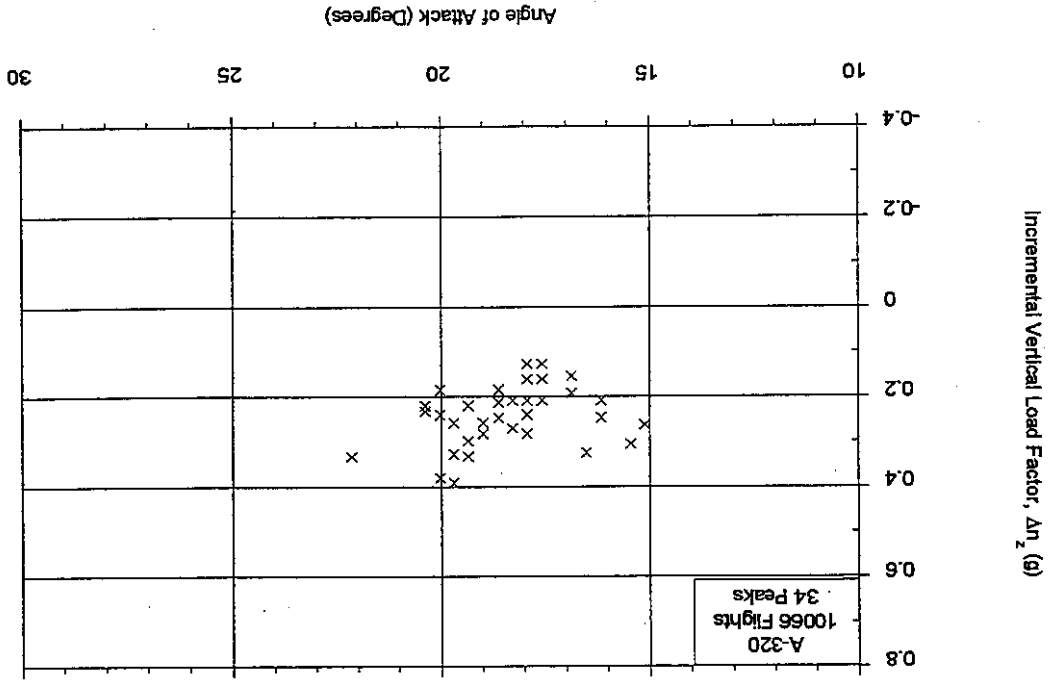


FIGURE A-41. MAXIMUM INCREMENTAL VERTICAL LOAD FACTOR VS. MAXIMUM ANGLE OF ATTACK DURING LIFTOFF, 170-180 KNOTS

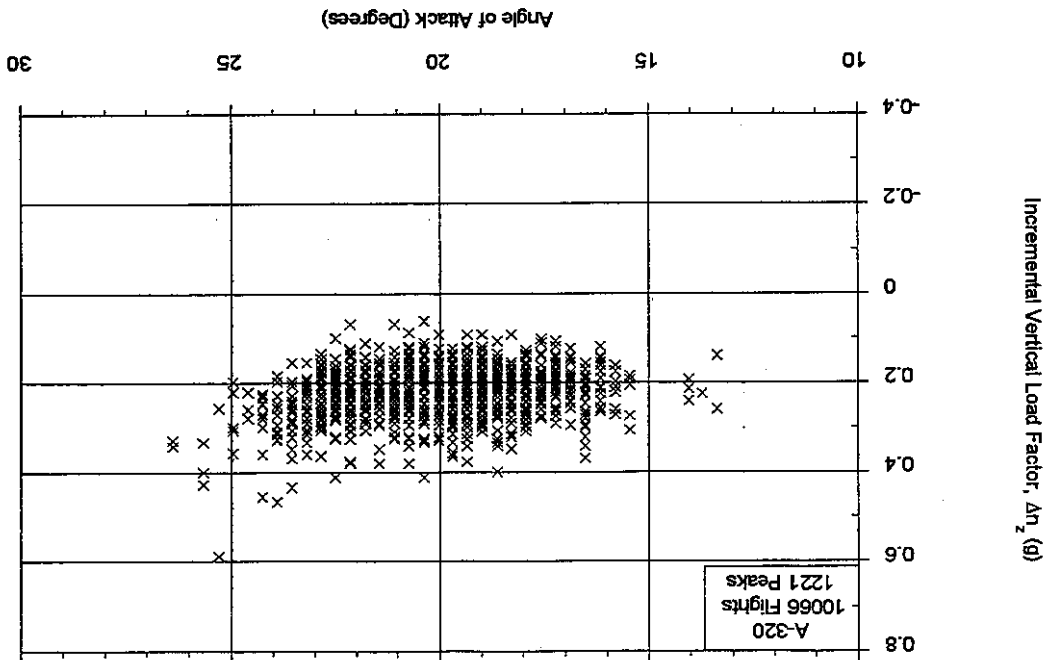


FIGURE A-46. MAXIMUM INCREMENTAL VERTICAL LOAD FACTOR AT TOUCHDOWN VS. MEAN WIND SPEED BEFORE TOUCHDOWN

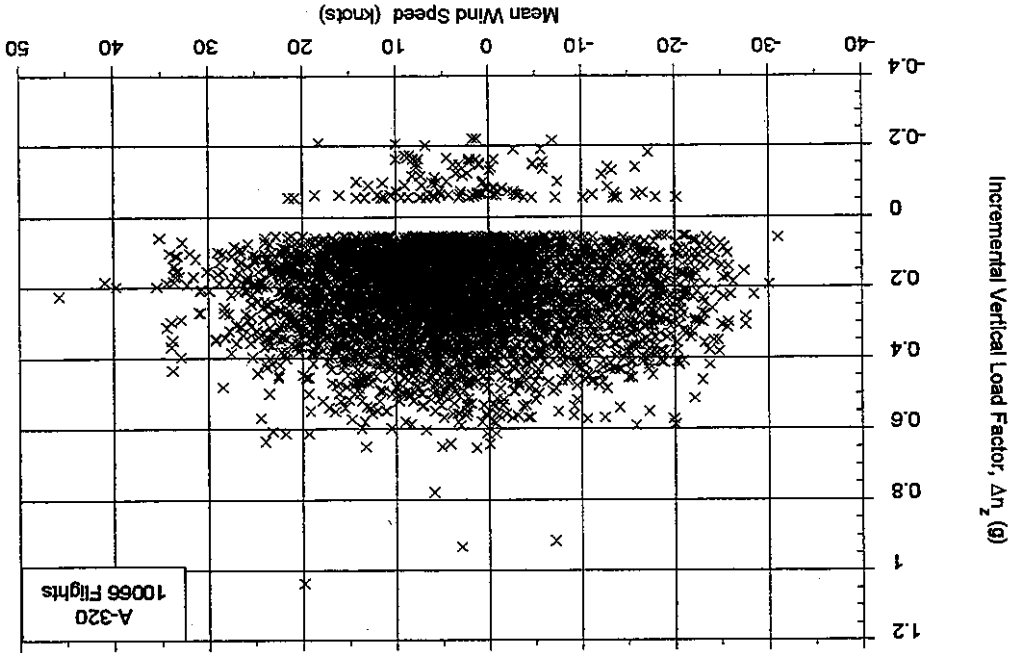
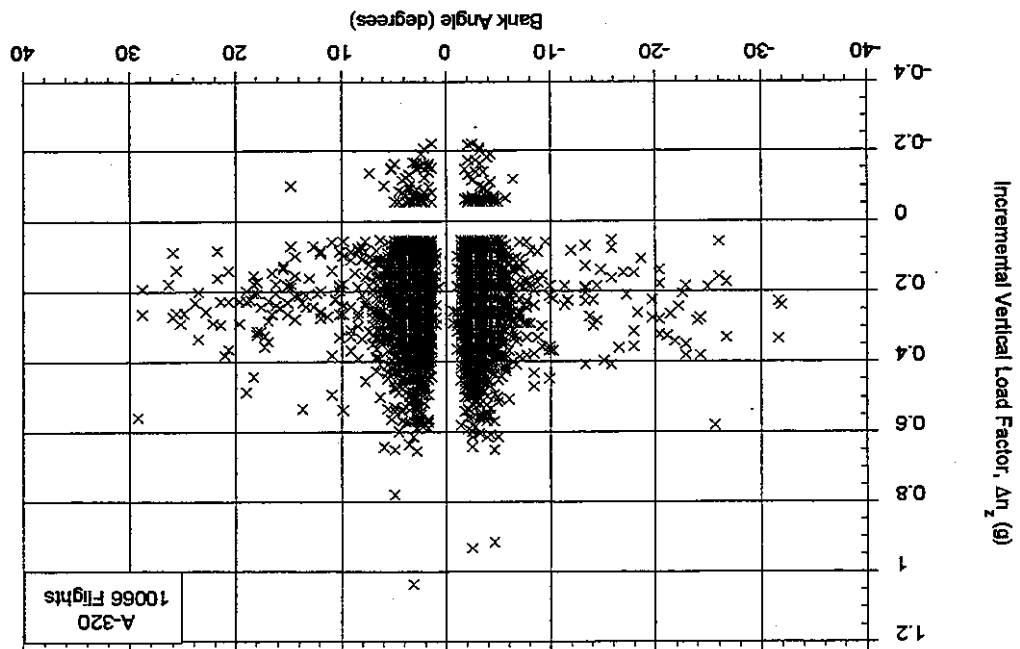


FIGURE A-45. MAXIMUM INCREMENTAL VERTICAL LOAD FACTOR AT TOUCHDOWN VS. MAXIMUM BANK ANGLE BEFORE TOUCHDOWN



RMS ACCELERATION (g)

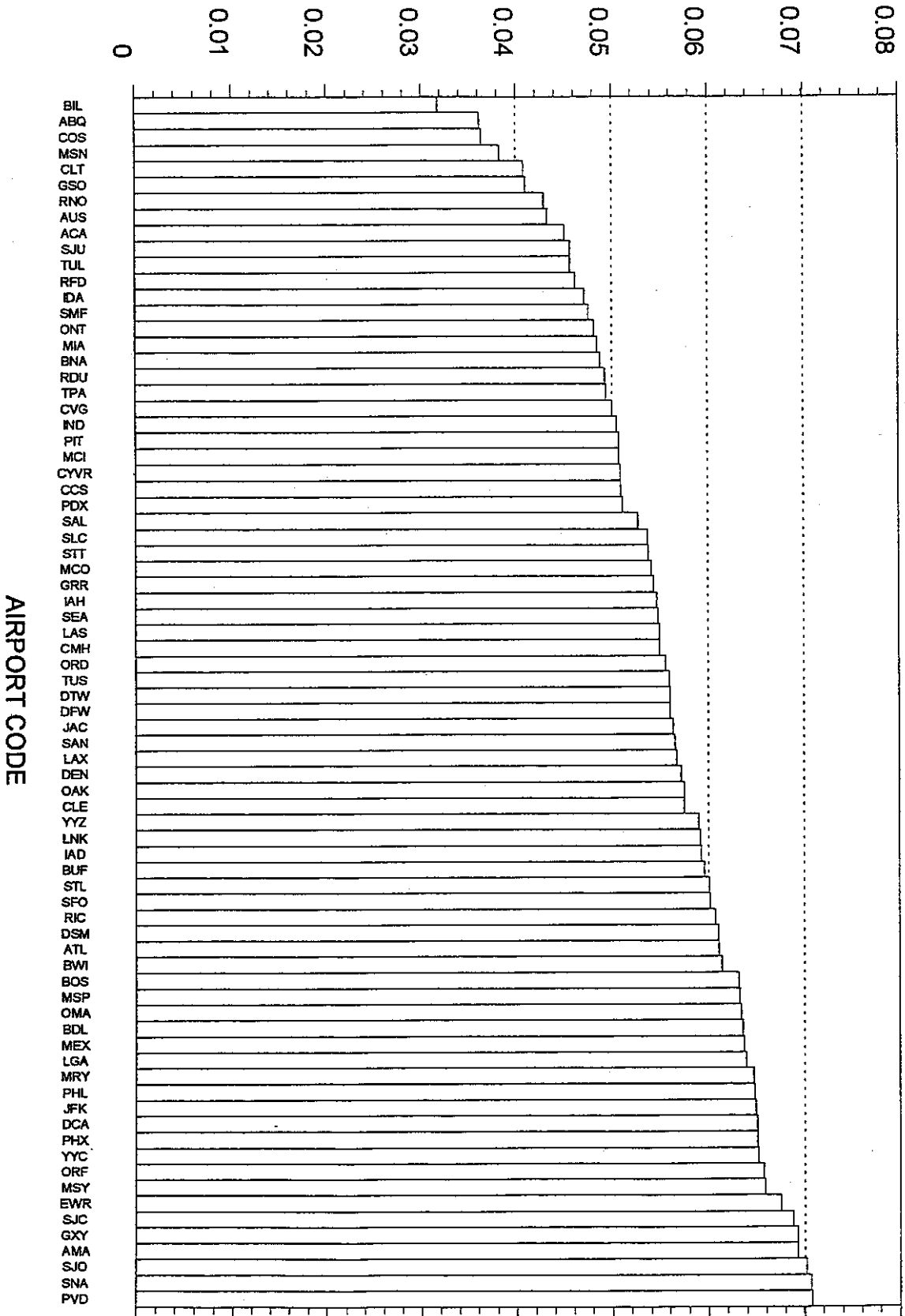


FIGURE A-49. AIRCRAFT RUNWAY ACCELERATION RESPONSE

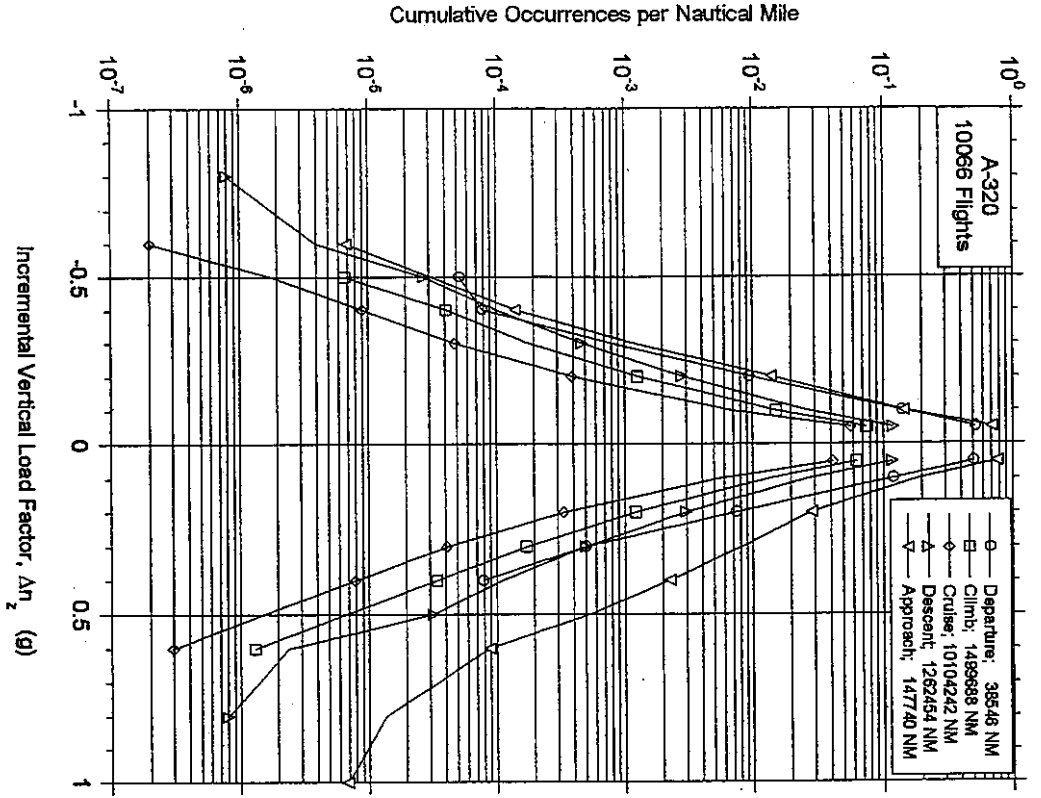


FIGURE A-52. CUMULATIVE OCCURRENCES OF INCREMENTAL VERTICAL GUST LOAD FACTOR PER NAUTICAL MILE BY FLIGHT PHASE

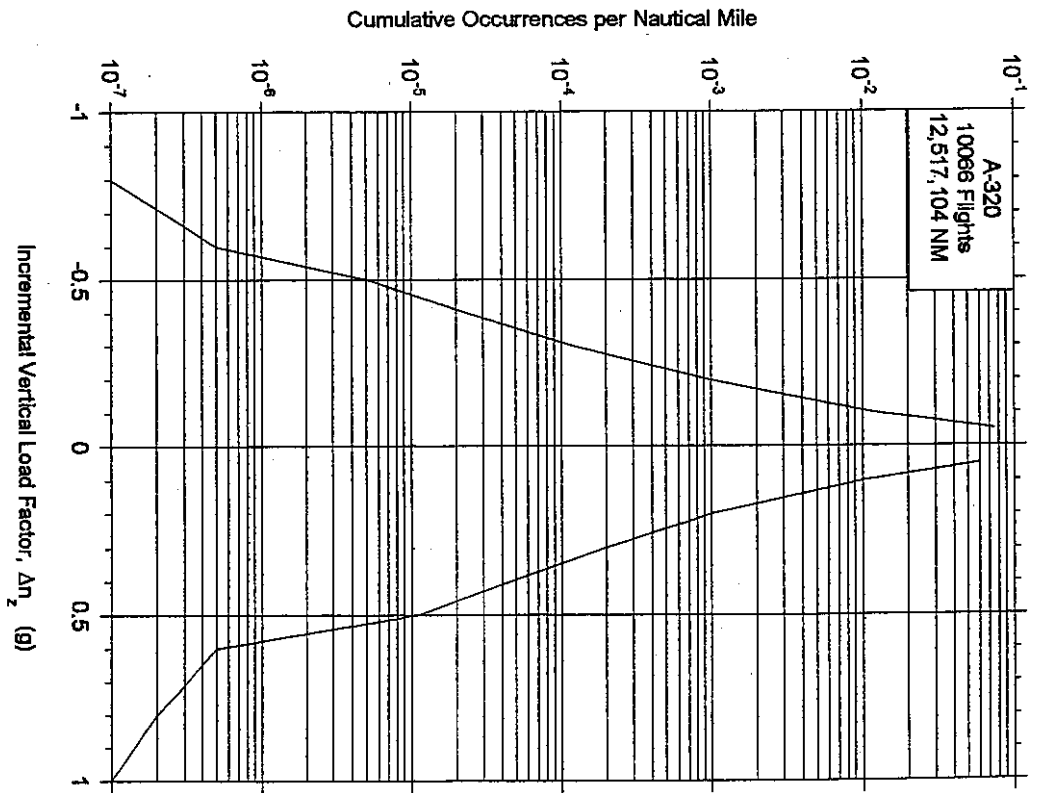


FIGURE A-53. CUMULATIVE OCCURRENCES OF INCREMENTAL VERTICAL GUST LOAD FACTOR PER NAUTICAL MILE, COMBINED FLIGHT PHASES

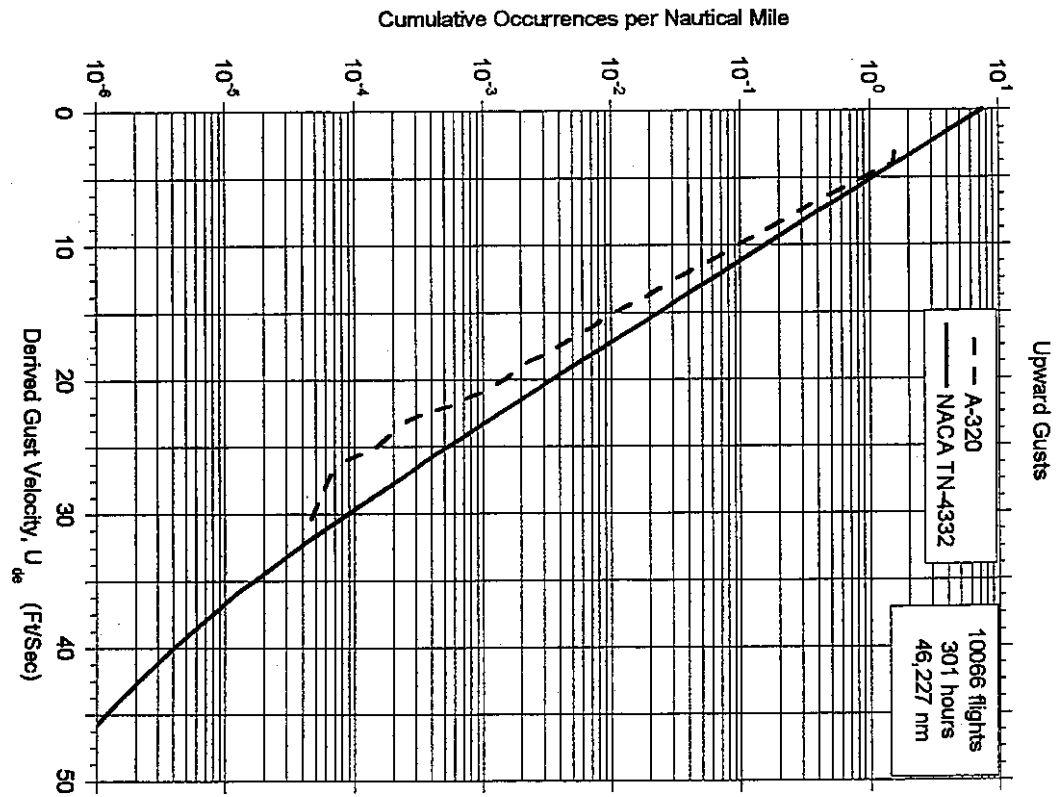
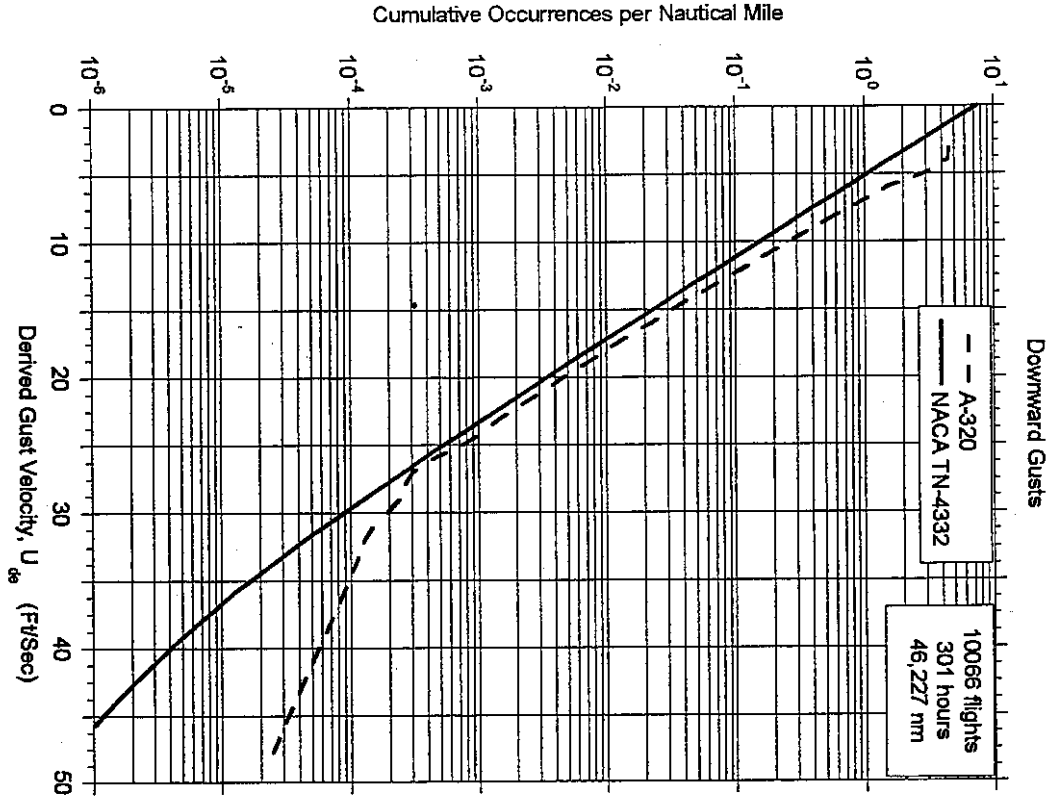


FIGURE A-55. CUMULATIVE OCCURRENCES OF DERIVED GUST VELOCITY PER NAUTICAL MILE, 500-1,500 FEET ABOVE AIRPORT

Flap Detent

10066 Flights	Detent 0	Detent 10	Detent 15	Detent 20	Detent 40
0	23419.5	146.2	305.1	121.3	98.5
0-1	5820.4	14.1	56.8	32.9	204.6
1-2	8.2	0.5	1.9	2.1	32.4
2-3	4.6	0.3	1.4	1.0	9.4
3-4	3.7	0.2	0.8	0.5	1.9
4-5	4.0	0.1	0.6	0.3	0.4
5-10	30.3	0.3	3.2	1.2	0.2
10-15	46.9	0.3	3.9	1.2	0.1
15-20	47.0	0.3	4.6	1.3	0.1
20-25	148.2	1.1	14.2	3.7	0.1
25-30	97.8	1.0	10.4	2.8	0.0
30-35	13.4	0.3	2.5	1.0	0.0
35-40	57.9	1.2	9.5	3.4	0.0
40-45	10.9	0.2	2.0	0.6	0.0

Speed Brake Deflection (degrees)

FIGURE A-107. TOTAL HOURS OF COINCIDENT SPEED BRAKE DEFLECTION AND FLAP DETENT

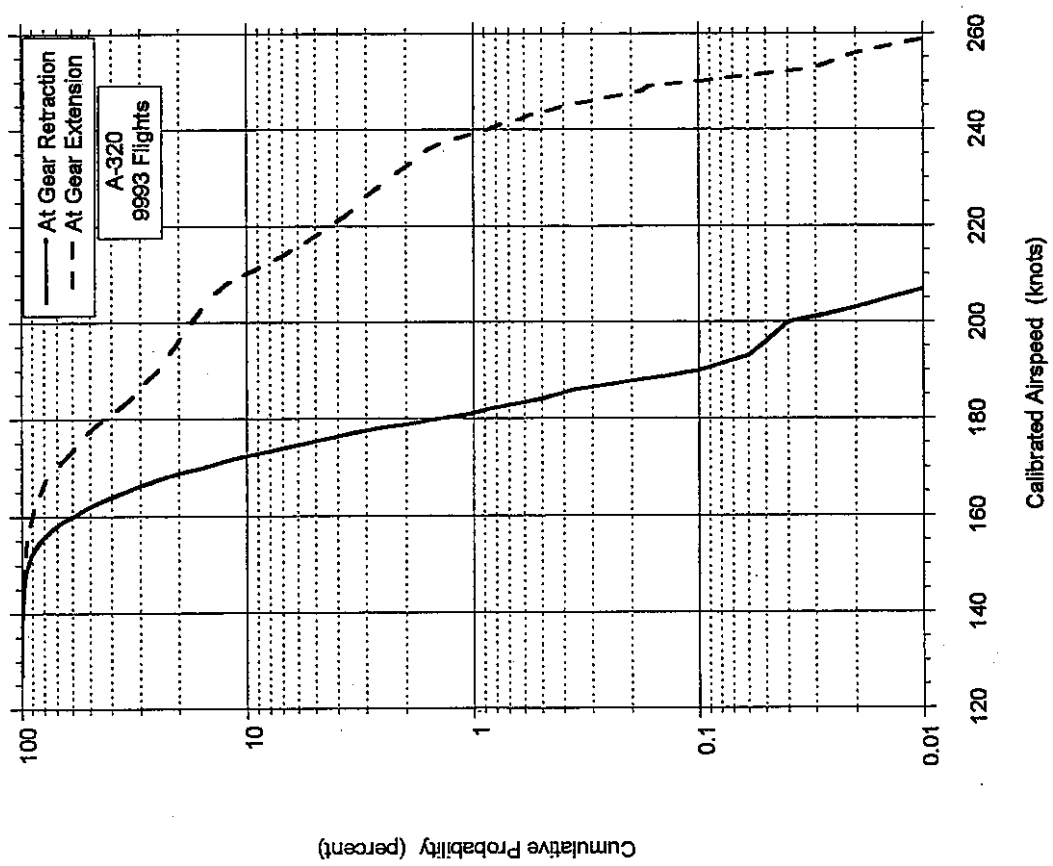


FIGURE A-110. CUMULATIVE PROBABILITY OF SPEED AT LANDING GEAR RETRACTION AND EXTENSION

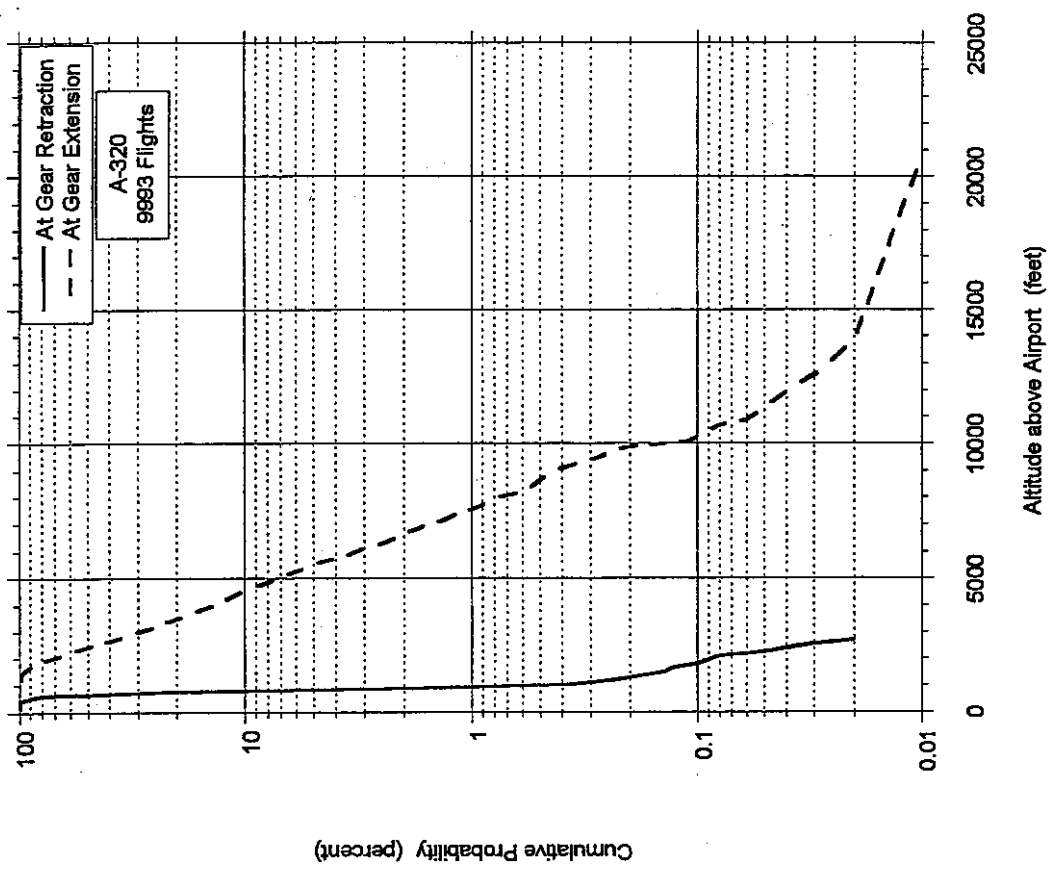


FIGURE A-111. CUMULATIVE PROBABILITY OF ALTITUDE ABOVE AIRPORT AT LANDING GEAR RETRACTION AND EXTENSION

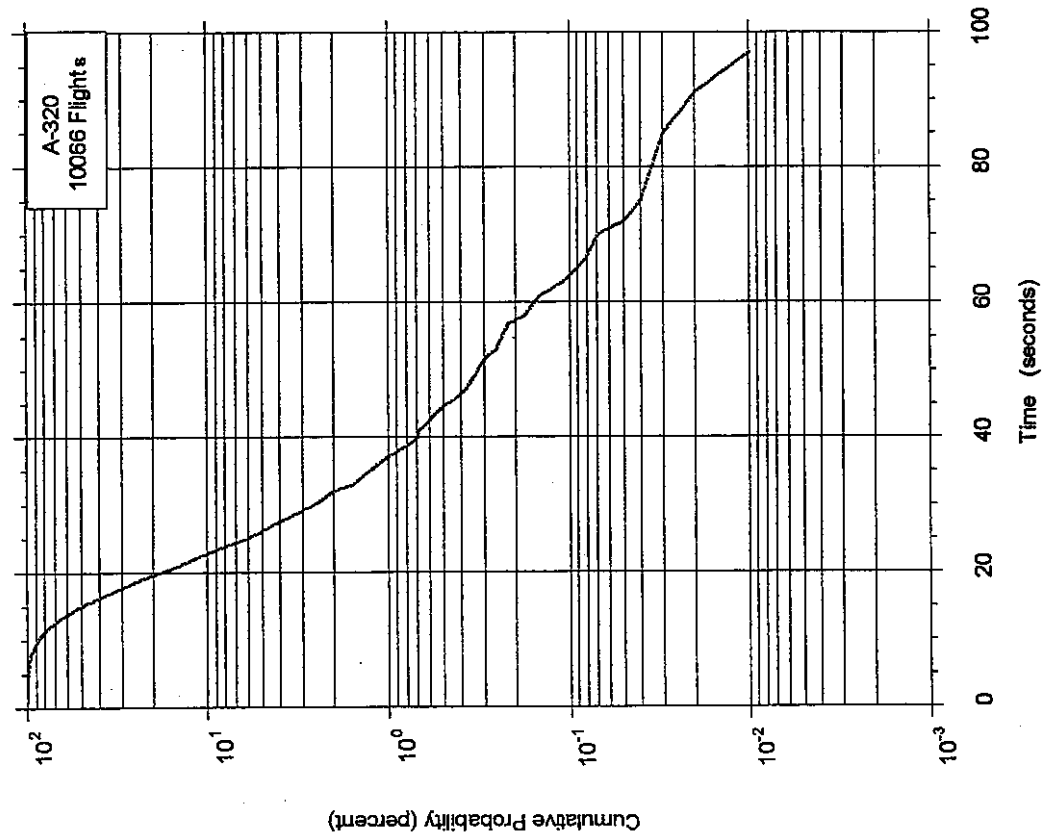


FIGURE A-114. CUMULATIVE PROBABILITY OF TIME WITH THRUST REVERSERS DEPLOYED

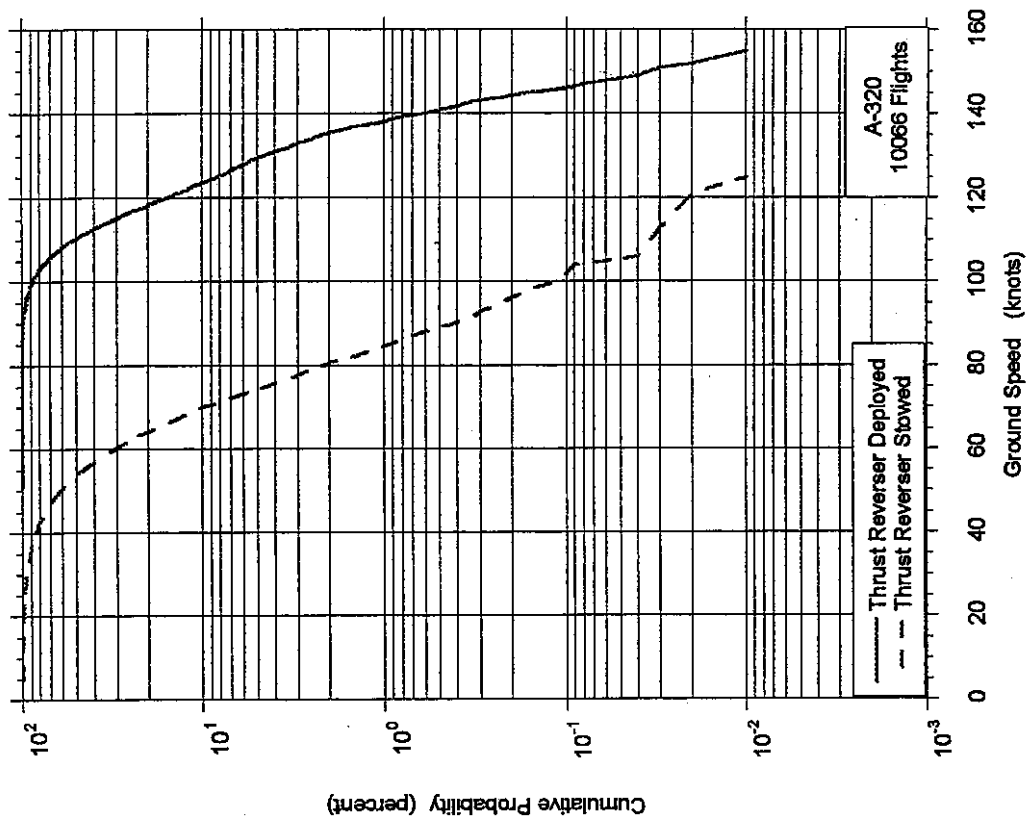


FIGURE A-115. CUMULATIVE PROBABILITY OF SPEED AT THRUST REVERSER DEPLOYMENT AND STOWAGE

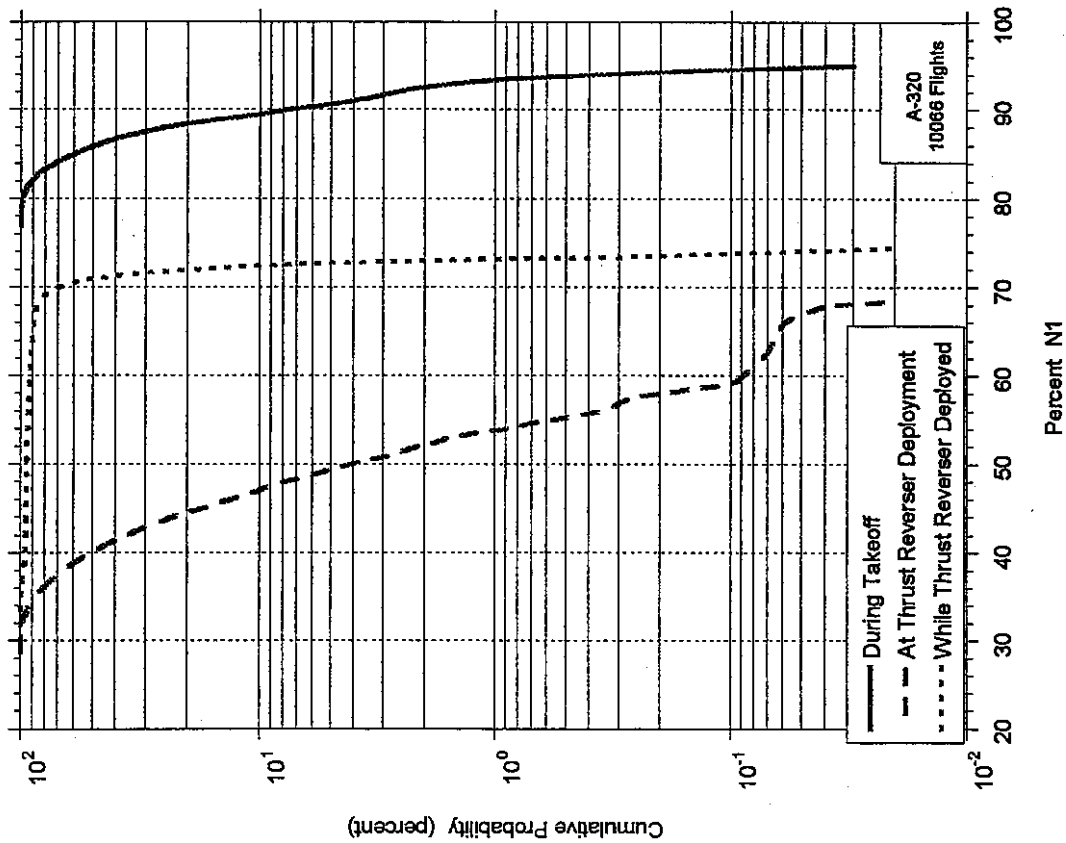
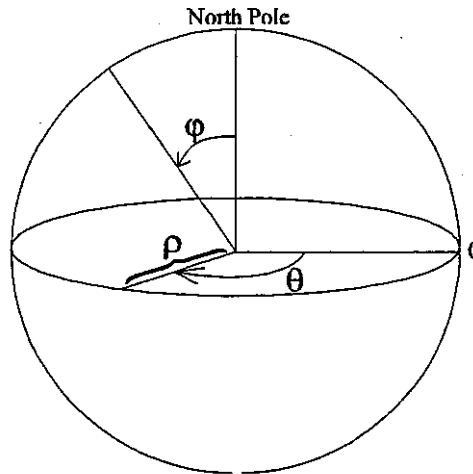


FIGURE A-118. CUMULATIVE PROBABILITY OF PERCENT OF N<sub>1</sub> DURING TAKEOFF, AT THRUST REVERSER DEPLOYMENT, AND DURING THRUST REVERSER DEPLOYMENT

## APPENDIX B—GREAT CIRCLE DISTANCE CALCULATION



Given:

Latitude and Longitude  
of Departure and  
Destination Airports

$\rho$  = distance from center  
 $\phi$  = angle from North Pole  
 $\theta$  = angle E/W of prime meridian

Procedure: (see sketch)

The standard mathematical system for spherical coordinates is shown, where three variables specify location:  $\rho$ ,  $\phi$ , and  $\theta$ .

Let  $a$  = Great Circle Distance in angular measure.

*Latitude* is measured away from the Equator ( $0^\circ$ ) to the North Pole ( $+90^\circ$ ) and the South Pole ( $-90^\circ$ ); whereas in the standard spherical coordinate system, the North Pole, Equator, and South Pole lie at  $0^\circ$ ,  $90^\circ$ , and  $180^\circ$ , respectively. Therefore,

$$\phi = 90^\circ - \text{latitude}$$

transforms latitude readings into equivalent angles ( $\phi$ ) in the standard spherical coordinate system.

Then

$$b = 90^\circ - \text{Latitude}_{\text{Dep}}$$

$$c = 90^\circ - \text{Latitude}_{\text{Des}}$$

where  $b$  and  $c$  are values of  $\phi$  for the departure and destination locations, respectively.

